

1 **Abstract**

2 We present a comprehensive study of a water-soluble substance from the class of triazine
3 derivatives alkylating agents. The performed physicochemical investigations of this cytostatic
4 drug's aqueous solutions include the measurements of density, viscosity, speed of sound,
5 refraction index, stability, solubility, distribution between water and octan-1-ol, as well as
6 electronic structure calculations and molecular dynamics modelling. Biologically, the substance
7 was investigated for its cytotoxicity as well as *in vitro* (on Capan-2 and SK-MEL-1 cell lines) and
8 *in vivo* (transplantable Ehrlich ascites carcinoma model) therapeutic activity.

9 **Keywords:** Cytostatic Agent; Solutions; Cytotoxicity; Ehrlich ascites carcinoma; Electronic
10 structure; Molecular Dynamics.

11

1 **1. Introduction**

2 This work continues our research on [5-[[4,6-*bis*(aziridin-1-yl)-1,3,5-triazin-2-
3 yl]amino]-2,2-dimethyl-1,3-dioxan-5-yl]methanol (substance (a)) from the group of alkylating
4 agents of the class of triazine derivatives (Fig. 1) [1]. 1,3,5-Triazine derivatives such as
5 Altretamine (1) [2], Tretamine (2) [3], and Azacitidine (3) [4] (Fig. 2) are used as selective
6 anticancer drugs against ovarian cancer [5], acute myeloid leukaemia [6], and chronic
7 myelomonocytic leukaemia [7]. Varying the substituents at the heterocycle (triazine) allows to
8 change the properties of the compound [8] with potentially advantageous medical effects.

9 Substance (a) was synthesised, investigated, and subsequently approved for medical use
10 in the 1980s as an antineoplastic agent for the treatment of ovarian, breast, lung, kidney, liver
11 cancers and for the prevention of regional metastasis in oral cancer [9–12]. In [13] it was shown
12 that substance (a) is effective against abdominal carcinomatosis in animals. A detailed study of the
13 mechanisms of action allowed to conclude that substance (a) is a small molecule from the class of
14 alkylating agents. It is characterised by both resorptive and contact antitumour effects and it can
15 be used for systemic and local chemotherapy, for endolymphatic chemotherapy, and
16 chemoembolisation [14].

17 Previously, our group obtained data on biocompatibility and biological activity of
18 substance (a). The data indicate high haemocompatibility, however, low affinity for human serum
19 albumin may lead to cytotoxicity. Binding of substance (a) to deoxyribonucleic acid investigated
20 by calorimetric titration, spectrophotometric method, and circular dichroism spectroscopy shows
21 that substance (a) exhibits a mixed mechanism of action. Its interaction with DNA leads to the
22 formation of covalent bonds, as evidenced by the high value of the binding constant ($K_b =$
23 $3.44 \cdot 10^7 \text{ M}^{-1}$). Experiments to study the kinetics of substance (a) interaction with DPPH, trapping
24 of NO radicals, and photobleaching of Radachlorin show that it exhibits pronounced antioxidant
25 activity. Cytotoxicity studies in cell lines (non-small cell lung cancer A-549, glioblastoma T98G,
26 ovarian teratocarcinoma PA-1, pancreatic cancer PANC-1, and liver adenocarcinoma SK-HEP-1)
27 showed a dose-dependent decrease in cell survival. The greatest effect was revealed in the case of

1 the A-549 cell line. Thus, we concluded that the cytotoxic effect of substance (a) may be due to
2 the change of antioxidant-prooxidant balance in tumour cells and damage to DNA molecules.

3 This work is dedicated to a comprehensive physicochemical study of substance (a)
4 aqueous solutions, namely, density, speed of sound, viscosity, refractive index, solubility, stability,
5 as well as the study of structural and dynamic characteristics in the binary system substance (a)–
6 H₂O. The physicochemical properties of a drug's aqueous solutions are extremely important in
7 revealing the mechanism of its action [15–24]. For example, data on densities, speed of sound,
8 viscosities allow to make conclusions about intermolecular interactions in solution, which, in turn,
9 can determine the mechanism of the drug's biological action. The viscosity of drug containing
10 systems is important for understanding the haemocompatibility of the test substance. The
11 distribution coefficient allows to predict the permeability through tissue and cellular barriers, as
12 well as the biodistribution of the drug. Stability studies are essential for understanding the
13 pharmacokinetics, pharmacodynamics, toxicokinetics, and metabolic stability of a drug.
14 Formulating dosage forms requires the knowledge of the active substance's compatibility with
15 water and aqueous solutions.

16 **2. Experimental part**

17 **2.1. Reagents**

18 The reagents used for conducting the experiments are listed in Table S1 of Supplementary
19 Material.

20 **2.2. Identification methods**

21 ¹H and ¹³C {¹H} NMR spectra were recorded on a Bruker Avance III 400 instrument
22 (400.13 MHz for ¹H and 100.61 MHz for ¹³C) in D₂O or in DCl, at 25°C. High resolution mass
23 spectral analysis was performed using Shimadzu 9030 and Bruker Daltonik GmbH 'MaXis'
24 instruments. ¹H and ¹³C {¹H} NMR spectra for substance (a) are in good agreement with
25 previously published data in ref. [1].

26 [5-[[4,6-*bis*(aziridin-1-yl)-1,3,5-triazin-2-yl]amino]-2,2-dimethyl-1,3-dioxan-5-
27 yl]methanol. ¹H NMR (400 MHz, D₂O, **after 1 h, pH = 7**), δ: 4.15 (d, *J* = 12.3 Hz, 2H, CH₂), 3.94

1 (d, $J = 12.3$ Hz, 2H, $\underline{\text{CH}_2}$), 3.88 (s, 2H, 2 $\underline{\text{CH}}$), 2.33 (s, 8H, 4 $\underline{\text{CH}_2}$), 1.42 (d, $J = 6.1$ Hz, 6H, 2 $\underline{\text{CH}_3}$).
2 HRMS (ESI⁺), m / z : 323.1826 [M+H]⁺, [C₁₄H₂₃N₆O₃]⁺. Calculated [M+H]⁺: 323.1828 (see Fig.
3 S1 of the Supplementary Material).

4 ¹H NMR (400 MHz, D₂O, **after 24 h, pH = 7**), δ : 4.17 (d, $J = 12.3$ Hz, 2H, $\underline{\text{CH}_2}$), 3.97 (d,
5 $J = 12.3$ Hz, 2H, $\underline{\text{CH}_2}$), 3.90 (s, 2H, 2 $\underline{\text{CH}}$), 2.36 (s, 8H, 4 $\underline{\text{CH}_2}$), 1.44 (d, $J = 6.1$ Hz, 6H, 2 $\underline{\text{CH}_3}$).
6 HRMS (ESI⁺), m / z : 323.1826 [M+H]⁺, [C₁₄H₂₃N₆O₃]⁺. Calculated [M+H]⁺: 323.1828 (see Fig.
7 S2 of the Supplementary Material).

8 NMR data of substance (a) in acidic and alkaline media was obtained as follows:

9 [5-[[4,6-*bis*(aziridin-1-yl)-1,3,5-triazin-2-yl]amino]-2-(hydroxymethyl)propane-1,3-diol.

10 ¹H NMR (400 MHz, DCl, **after 1 h, pH = 3**), δ : 3.86–3.78 (m, 6H, 3 $\underline{\text{CH}_2}$), 3.69 (q, $J = 5.8$ Hz,
11 4H, 2 $\underline{\text{CH}_2}$), 2.16 (s, 8H, 4 $\underline{\text{CH}_2}$). HRMS (ESI⁺), m / z : 283.1512 [M+H]⁺, [C₁₁H₁₉N₆O₃]⁺.
12 Calculated [M+H]⁺: 283.1513 (see Fig. S3 of the Supplementary Material).

13 [5-[[4,6-*bis*(aziridin-1-yl)-1,3,5-triazin-2-yl]amino]-2-(hydroxymethyl)propane-1,3-diol.

14 ¹H NMR (400 MHz, D₂O, **after 1 h, pH = 4**), δ : 3.70–3.62 (m, 6H, 3 $\underline{\text{CH}_2}$), 3.54 (s, 4H, 2 $\underline{\text{CH}_2}$),
15 2.07 (s, 8H, 4 $\underline{\text{CH}_2}$).

16 [5-[[4,6-*bis*(aziridin-1-yl)-1,3,5-triazin-2-yl]amino]-2,2-dimethyl-1,3-dioxan-5-
17 yl]methanol. ¹H NMR (400 MHz, D₂O, **after 1 h, pH = 10**), δ : 4.15 (d, $J = 12.3$ Hz, 2H, $\underline{\text{CH}_2}$),
18 3.94 (d, $J = 12.3$ Hz, 2H, $\underline{\text{CH}_2}$), 3.88 (s, 2H, 2 $\underline{\text{CH}}$), 2.33 (s, 8H, 4 $\underline{\text{CH}_2}$), 1.42 (d, $J = 6.1$ Hz, 6H,
19 2 $\underline{\text{CH}_3}$).

20 Single crystals of substance (a) were selected using an optical microscope, encased in an
21 oil-based cryoprotectant and mounted on cryoloops (Fig. 3). The measurement was carried out
22 using a Rigaku Oxford Diffraction XtaLAB SuperNova diffractometer with an HyPix3000 CCD
23 area detector operated with monochromated microfocussed CuK α radiation ($\lambda[\text{CuK}\alpha] = 1.54184$
24 Å). Experimental data processing was carried out using CrysAlisPro software. The structures were
25 solved by direct methods and refined using the SHELX [25,26] program incorporated in the
26 OLEX2 [27] software package.

1 **2.3. Study of physicochemical properties of substance (a) aqueous solutions**

2 The temperature and concentration dependencies of physicochemical properties in the
3 binary system substance(a)–water were studied using following apparatus: (i) Anton Paar DSA
4 5000 (Austria) for measuring density and speed of sound; (ii) Lovis 2000 M Anton Paar
5 microviscometer (Austria) for measuring viscosity; (iii) Automatic Multi Wavelengths
6 Refractometer Abbemat WR/MW (Austria) for measuring refraction index. The description of
7 experimental techniques, as well as metrological characteristics are presented elsewhere [28–40].

8 **2.3.1. Solubility of substance (a) in aqueous solutions**

9 The measurements of the solubility of substance (a) in water at atmospheric pressure
10 were carried out in the temperature range $T = 293.15\text{--}318.15$ K with isothermal saturation method
11 for 12 h using a thermostatically controlled shaker LAUDA ET 20 with shaking frequency of 80
12 Hz. The temperature was measured with an error of 0.1 K. The required volume (about 5 cm^3) was
13 taken from the heterogeneous system at atmospheric pressure for spectrophotometric analysis.
14 Then the liquid phase was separated by vacuum filtration for spectrophotometric analysis.

15 The concentration of substance (a) in a saturated solution was determined
16 spectrophotometrically using an SF-2000 spectrophotometer (Russia). Fig. 4 presents the
17 electronic spectrum of substance (a) at $\lambda = 200\text{--}400$ nm. Fig. 5 demonstrates the agreement with
18 Beer–Lambert–Bouguer law ($R^2 = 0.989$) at $\lambda = 220$ nm. For substance (a) concentration
19 determination in a saturated solution, the following equation was applied (at optical wavelength
20 equal to 1 cm):

$$21 \quad C = 0.049 \cdot A(220\text{ nm}), \quad (1)$$

22 where C is the volume concentration of substance (a) ($\text{g}\cdot\text{dm}^{-3}$), $A(220\text{ nm})$ is the absorbance at λ
23 $= 220$ nm.

24 The composition of the equilibrium crystalline hydrate of substance (a) was determined
25 by the thermogravimetric method using NETZSCH TG 209 F1 Libra thermogravimetric analyser
26 (Germany) in the temperature range of $40\text{--}600$ °C in nitrogen atmosphere and heating rate of
27 $5\text{ °C}\cdot\text{min}^{-1}$. Fig. 6 presents the thermogram of the crystalline hydrate of substance (a).

1 **2.3.2. Stability of substance (a) aqueous solutions**

2 The hydrolysis reaction of substance (a) in D₂O was studied at 25 °C by recording the ¹H
3 NMR spectra of the reaction mixture on Bruker Avance III 400 (400.13 MHz) for 24 h in automatic
4 mode with one spectrum recording every 30 min.

5 To study the stability of substance (a) in an acidic medium (pH = 3, 4), 20 mg of substance
6 (a) was dissolved in 40 ml of aqueous solutions of hydrochloric acid. The resulting solution was
7 stirred at room temperature for 45 min. At the end of the reaction, the solvent was removed under
8 standard conditions. The product was air dried.

9 To study the stability of substance (a) in an alkaline medium (pH = 10), 20 mg of substance
10 (a) was dissolved in 40 ml of an aqueous solution of 0.1 M NaOH. The resulting solution was
11 stirred at room temperature for 1 h. At the end of the reaction, the solvent was removed under
12 standard conditions. The product was air dried.

13 **2.3.3. Distribution coefficient**

14 The study of the distribution of substance (a) in the octan-1-ol–H₂O system was carried out
15 in a shaker-thermostat LAUDA ET 20 (shaking frequency of 80 Hz). The temperature was
16 maintained within the accuracy of 0.1 K (95 % confidence interval), the time of the experiment
17 was 5 h. For the experiment, the solution of substance (a) was prepared ($C = 1 \text{ g}\cdot\text{dm}^{-3}$) in deionised
18 water (electrical conductivity $5.5\cdot 10^{-6} \text{ S}\cdot\text{m}^{-1}$) to which an equal volume of octan-1-ol was added
19 (25.0 ml). After reaching the equilibrium, an aliquot of the lower aqueous phase was taken. While
20 dipping the pipette into the two-phase system, air was carefully blown through it to prevent the
21 upper organic phase from entering the pipette. The concentration of substance (a) in the aqueous
22 phase was measured by the spectrophotometric method using SF-2000 spectrophotometer at the
23 wavelength $\lambda = 220 \text{ nm}$ according to Eq. 1. In total, five parallel measurements were carried out.

24 **2.3.4. Membrane mitochondrial potential measurement**

25 PANC-1 cells were trypsinised and washed with PBS (phosphate-buffered saline),
26 containing 10 % fetal bovine serum (FBS). Afterwards, the cells were resuspended in a mixture of
27 PBS, 5 % FBS and 50 mM KCl. After the incubation of the cells with MitoTracker® Orange

1 CMTMRos fluorescent dye (500 nM) at 37 °C for 30 min, they were rinsed with PBS and plated
2 into a black 96-well plate (80,000 cells per well). The concentration of substance (a) and
3 doxorubicin in final suspensions were equal to 100 μM. For the dissipation of the proton gradient,
4 10 μM of FCCP (carbonyl cyanide-*p*-trifluoromethoxyphenylhydrazone) was added. The
5 measurements of fluorescence was carried out using microplate reader (TECAN Instrument,
6 Austria) at the excitation/emission wavelength of 554/576 nm.

7 **2.3.5. Computer simulation**

8 The study of substance (a) at the atomic/molecular level was started with the calculations
9 of the electronic structure of the molecule. DFT calculations using DMol³ tool from Materials
10 Studio software package produced charges according to the Mulliken scheme. The calculations
11 were carried out with the PBE, PW91, HCTH functionals and the DNP atomic basis (4.4). To
12 account for the environment (vacuum, *n*-hexane, acetonitrile, water), the COSMO model was used.

13 The obtained charges were used to construct the electrostatic component of the force field
14 for classical Molecular Dynamics calculations. The short-range interactions were represented by
15 the Universal Force Field. Simulated systems consisted of one substance (a) molecule and three
16 thousand solvent molecules in the NVT ensemble. The calculation parameters were: 5 ns
17 simulation time, 298 K temperature, 1 fs integration step, Nosé–Hoover thermostat.

18 **2.4. *In vitro* investigation of substance (a)**

19 Substance (a) cytotoxicity towards pancreas adenocarcinoma (Capan-2) and skin
20 melanoma (SK-MEL-1) cell lines was carried out using MTT-assay. The experimental technique
21 is described elsewhere [1,41].

22 **2.5. *In vivo* investigation of substance (a) in a transplantable Ehrlich ascites carcinoma** 23 **murine model**

24 The study was carried out in 20 female BALB/c mice which were kept under
25 environmentally relevant conditions with a 12:12 light–dark cycle. Standard murine food and
26 water were provided *ad libitum*. The research was approved by the Local Ethics Committee of
27 Pavlov First Saint Petersburg State Medical University, and carried out in accordance with the

1 University guidelines and ethical standards as well as ARRIVE guidelines. After intraperitoneal
2 transplantation of Ehrlich ascites carcinoma, all animals were randomised into 2 groups, 10 mice
3 per group: control mice ($n = 10$) and mice with administrated substance (a) at the concentration of
4 $5 \text{ mg}\cdot\text{kg}^{-1}$ i. p. ($n = 10$). Substance (a) was administered once intraperitoneally, 48 h after the
5 tumour transplantation. The volume of the injected substance (a) 0.9 % sodium chloride solution
6 was 80 ml per kg. The control mice were injected i. p. with 0.9 % sodium chloride solution of the
7 same volume.

8 **3. Results and discussion**

9 **3.1. Identification**

10 Mass spectrometry and NMR spectroscopy data confirmed the composition and structure
11 of substance (a). The signals of the protons of the aziridine groups were found in the range 2.33–
12 2.36 ppm, and the signals at 1.42–1.44 ppm confirmed the presence of two CH_3 -groups in the
13 dioxane fragment.

14 Crystal Data for substance (a) $\text{C}_{14}\text{H}_{22}\text{N}_6\text{O}_3$ ($M = 322.37 \text{ g}\cdot\text{mol}^{-1}$) were the following:
15 triclinic, space group P-1 (no. 2), $a = 9.0771(2) \text{ \AA}$, $b = 9.0823(2) \text{ \AA}$, $c = 9.8721(2) \text{ \AA}$, $\alpha =$
16 $79.883(2)^\circ$, $\beta = 83.960(2)^\circ$, $\gamma = 72.365(2)^\circ$, $V = 762.38(3) \text{ \AA}^3$, $Z = 2$, $T = 100(2) \text{ K}$, $\mu(\text{CuK}\alpha) =$
17 0.846 mm^{-1} , $D_{\text{calc}} = 1.404 \text{ g/cm}^3$, 20099 reflections measured ($9.114^\circ \leq 2\theta \leq 152.508^\circ$), 3089
18 unique ($R_{\text{int}} = 0.0406$, $R_{\text{sigma}} = 0.0231$) which were used in all calculations. The final R_1 was 0.0373
19 ($I > 2\sigma(I)$) and wR_2 was 0.0989 (all data). Additional X-ray diffraction data for substance (a) are
20 presented in Tables S2–S5 of the Supplementary Material.

21 **3.2. Study of physicochemical properties of substance (a) aqueous solutions**

22 **3.2.1. Density of aqueous solutions of substance (a)**

23 The results of substance (a) aqueous solution density ($C = 0.025\text{--}10 \text{ g}\cdot\text{dm}^{-3}$, $T = 293.15\text{--}$
24 333.15 K) are shown in Table S6 and Fig. 7. The average molar volumes and partial molar volumes
25 of the solution components were obtained according to Eqs. 2 and 3:

$$26 \quad \bar{V} = \frac{V}{n_{\text{H}_2\text{O}} + n_a}, \quad (2)$$

$$1 \quad V_{\text{H}_2\text{O}} = \bar{V} - x_a \left(\frac{\partial \bar{V}}{\partial x_a} \right)_{T,P}, \quad V_a = \bar{V} - x_{\text{H}_2\text{O}} \left(\frac{\partial \bar{V}}{\partial x_{\text{H}_2\text{O}}} \right)_{T,P}. \quad (3)$$

2 where \bar{V} is the average molar volume, V is the volume of substance (a) aqueous solution; $n_{\text{H}_2\text{O}}, n_a$
 3 and $x_{\text{H}_2\text{O}}, x_a$ are the amounts of substance and molar fractions of the solution components,
 4 respectively, $V_{\text{H}_2\text{O}}$ and V_a are partial molar volumes of the solution components.

5 Figs. 8–10 present the concentration dependences of the average molar volume and the
 6 partial molar volumes in the temperature range $T = 293.15\text{--}333.15$ K. The results reveal that the
 7 dependence of substance (a) partial molar volume in the region of diluted solutions has a
 8 complicated shape: At low concentration up to $0.1 \text{ g}\cdot\text{dm}^{-3}$, the values of V_a slightly decrease. This
 9 fact shows that introducing little amount of substance (a) in the system leads to condensing and
 10 structuring of the solution.

11 3.2.2. Speed of sound of substance (a) aqueous solutions

12 Table S7 presents the values of the speed of sound in the substance (a)–H₂O system in the
 13 temperature interval $T = 278.15\text{--}323.15$ K. Isentropic compressibility (κ_S) was calculated
 14 according to Lalpaca equation (Fig. 11):

$$15 \quad \kappa_S = \rho^{-1} \cdot u^{-2}, \quad (4)$$

16 where ρ is the density of the solution, u is speed of sound.

17 Intermolecular interactions between water and substance (a) can be evaluated using the
 18 apparent specific isentropic compressibility ($\kappa_{S,\phi}$) [42–44]:

$$19 \quad \kappa_{S,\phi} = \frac{\kappa_{S_a} (1 + m_a)}{\rho m_a} - \frac{\kappa_{S_{\text{water}}}}{\rho_{\text{water}} m_a}, \quad (5)$$

20 where m_a is the molality of substance (a), κ_{S_a} and $\kappa_{S_{\text{water}}}$ are the isentropic compressibility of
 21 solution components, ρ and ρ_{water} are the density of solution components.

22 Fig. 12 shows the concentration dependences of the apparent specific isentropic
 23 compressibility in the studied temperature range. The analysis of the results obtained allows to
 24 state the following: (i) the value of $\kappa_{S,\phi}$ is positive in the entire concentration range. This fact

1 testifies to the high compressibility of water molecules in the binary system substance (a)–water
 2 in comparison with the one-component system. The obtained result is in good agreement with the
 3 data on the concentration dependences of the partial molar volume of substance (a) and confirms
 4 the fact of structuring and compaction of the solution in the region of low concentrations; (ii) a
 5 decrease in $\kappa_{S,\phi}$ with an increase in the concentration of the solute indicates that the compressibility
 6 of water molecules in the system under study approaches the compressibility of a pure solvent;
 7 (iii) it is obvious that an increase in temperature decreases the value of $\kappa_{S,\phi}$ due to the weakening
 8 of intermolecular interactions in the system.

9 **3.2.3. Viscosity of substance (a) aqueous solutions**

10 Table S8 presents data on the dynamic and kinematic viscosity in the binary system
 11 substance (a)–water in the temperature range $T = 293.15\text{--}333.15$ K. The kinematic viscosity was
 12 calculated according to Eq. 6 [45]:

$$13 \quad \eta_k = \frac{\eta}{\rho}. \quad (6)$$

14 The thermodynamic characteristics of viscous flow activation (ΔG , ΔH , ΔS , E_a) were
 15 calculated using Eyring's theory according to the following equations (see Table 1) [45]:

$$16 \quad \Delta G = RT \ln \frac{\eta V}{h N_A}, \quad (7)$$

$$17 \quad \Delta G = \Delta H - T \Delta S, \quad (8)$$

$$18 \quad \ln \eta = \ln A_s + \frac{E_a}{R} \frac{1}{T}, \quad (9)$$

$$19 \quad T_A = \frac{-E_a}{R \ln A_s}, \quad (10)$$

20 where ΔG , ΔH , and ΔS are Gibbs energy, enthalpy, and entropy of viscous flow, A_s is the pre-
 21 exponential entropic factor corresponding to the viscosity at the infinite temperature, E_a is the
 22 activation energy of the transition state, T_A is the activation temperature, R is the molar gas
 23 constant, T is the absolute temperature.

1 The analysis of the obtained values of the thermodynamic functions of viscous flow
 2 activation allows to conclude the following: (i) the enthalpy values are stable and positive over the
 3 entire concentration range. This fact indicates the presence of specific interactions in solution; (ii)
 4 the stability of entropy values is observed over the entire concentration range. The negative
 5 definiteness of entropy indicates ordering in solution associated with the formation of an activated
 6 complex. This fact indicates the interaction between the molecules of the solute and the solvent.

7 The temperature dependences of the dynamic viscosity of aqueous solutions of substance
 8 (a) were described using the van't Hoff equation (Fig. 13):

$$9 \quad \gamma_{\eta}^{\frac{\Delta T}{T}} = \frac{\eta_{T-\Delta T}}{\eta_T} = 1.21 \pm 0.05, \quad (11)$$

10 where γ_{η} is the van't Hoff viscosity coefficient.

11 The analysis of Fig. 13 shows that the van't Hoff temperature coefficient is constant over
 12 the studied temperature range.

13 Fig. 14 shows the results of applying the three-parameter Vogel–Fulcher–Tammann (VFT)
 14 equation [46] to describe the temperature dependences of the dynamic viscosity in the binary
 15 system substance (a)–water. Table 2 summarises the values of the parameters for the VFT
 16 equation, as well as the average absolute deviation (AAD) and standard deviation (SD) values.

17 **3.2.4. Refractions of substance (a) aqueous solutions**

18 Table S9 presents the experimental data on the refractive indices of substance (a) solutions
 19 (n_D) at $C = 0.01\text{--}25 \text{ g}\cdot\text{dm}^{-3}$ and in the temperature interval $T = 293.15\text{--}333.15 \text{ K}$.

20 Specific and molar refractions of solutions were calculated using Eqs. 12, 13:

$$21 \quad r = \left(\frac{n_D^2 - 1}{n_D^2 + 2} \right) \cdot \frac{1}{\rho}, \quad (12)$$

$$22 \quad R = \left(\frac{n_D^2 - 1}{n_D^2 + 2} \right) \cdot \frac{\overline{M}}{\rho}, \quad (13)$$

1 where r and R are the specific and molar refractions, \overline{M} is the average molar mass of the solution
 2 ($\overline{M} = x_{\text{H}_2\text{O}} \cdot M_{\text{H}_2\text{O}} + x_{\text{a}} \cdot M_{\text{a}}$). We did not use the experimental data on refraction indices at low
 3 concentration region ($x_{\text{a}} < 1.4 \cdot 10^{-4}$) due to low accuracy (see Table 3).

4 The specific (r) and molar (R) refractions of substance (a) were calculated according to
 5 Eqs. 14, 15:

$$6 \quad r = (r_{\text{H}_2\text{O}} \cdot w_{\text{H}_2\text{O}} + r_{\text{a}} \cdot w_{\text{a}}) \cdot \frac{1}{100}, \quad (14)$$

$$7 \quad R = R_{\text{H}_2\text{O}} \cdot x_{\text{H}_2\text{O}} + R_{\text{a}} \cdot x_{\text{a}}, \quad (15)$$

8 where r_i , R_i are specific and molar refractions of the solution components, w_i , x_i are the mass and
 9 molar fractions of the solution components (see Table 3).

10 Additionally, the substance (a) molar refraction was estimated using the Eisenlohr (Eq. 16)
 11 and Vogel (Eq. 17) additivity rules [47]:

$$12 \quad R^{\text{add}} = 14R_{\text{C}} + 22R_{\text{H}} + R_{\text{O(OH)}} + 2R_{\text{O(R-O-R')}} + R_{\text{N(R}_2\text{NH)}} + 2R_{\text{N(R}_3\text{N)}} + 3R_{\text{N(C-N=C)}} \approx 83.345 \text{ cm}^3 \cdot \text{mol}^{-1}, \quad (16)$$

$$13 \quad R^{\text{add}} = 20R_{\text{C-H}} + 11R_{\text{C-N}} + 7R_{\text{C-C}} + 5R_{\text{C-O}} + 3R_{\text{C=N}} + R_{\text{O-H}} + R_{\text{N-H}} \approx 82.262 \text{ cm}^3 \cdot \text{mol}^{-1}. \quad (17)$$

14 The specific refraction of substance (a) was determined using Eq. 18:

$$15 \quad r^{\text{add}} = \frac{R^{\text{add}}}{M_{\text{a}}}. \quad (18)$$

16 The obtained values are equal to $0.259 \text{ cm}^3 \cdot \text{g}^{-1}$ (calculated from the molar refractions
 17 according to Eisenlohr rule) and $0.255 \text{ cm}^3 \cdot \text{g}^{-1}$ (calculated from the molar refractions according to
 18 Vogel rule).

19 The comparison between experimental and calculated data on specific (a) and molar
 20 refractions (b) are presented in Fig. 15. One can see good correspondence between the results.

21 **3.2.5. Correlation of physicochemical properties of substance (a) aqueous solutions**

22 T - C data on investigated physicochemical properties of substance (a) aqueous solutions
 23 (density, speed of sound, viscosity, and refraction index) were fitted using Eq. 19:

$$24 \quad M = a + \sum_{i=1}^4 b_i \cdot T^i + \sum_{j=1}^4 c_j \cdot C^j, \quad (19)$$

1 where M is the property under correlation, a , b_i , c_j ($i, j = 1-4$) are the fitting parameters obtained
2 using the least-square method in OriginLab software (Table 4, Fig. 16).

3 **3.3. Substance (a) solubility**

4 Fig. 17 presents the experimental values of the solubility of substance (a) in water ($T =$
5 293.15–318.15 K). It can be seen that substance (a) is well soluble in water. The solubility values
6 varied in the range 26.3–43.0 g·dm⁻³ in the studied temperature range. It is clearly seen that the
7 temperature dependence of solubility has a sigmoidal form. At the same time, the solubility rises
8 with temperature increase. This fact determines that dissolution of substance (a) in water is
9 accompanied with an endothermic effect. Conducted thermogravimetric analysis shows that the
10 equilibrium solid phase with saturated solution is a crystalline hydrate of substance (a) of
11 composition C₁₄H₂₂N₆O₃·3H₂O.

12 **3.4. Study of the stability of substance (a) in aqueous solutions by NMR spectroscopy**

13 The effect of the solvent on the stability of substance (a) was investigated by measuring
14 the kinetics of the reaction by ¹H NMR spectroscopy. During the experiment, the intensity did not
15 decrease, and displacement of the signals corresponding to the protons of the parent compound
16 was not recorded. Within 24 h, no changes were found in the original spectra. Fig. 18 shows the
17 fragments of ¹H NMR spectra recorded at regular intervals in an automatic mode. There is no
18 visible shift of signals or decrease in their intensity over time. Thus, it can be concluded that
19 substance (a) is stable at pH = 7 at least for 24 h.

20 In addition, we investigated the influence of pH on the stability of substance (a) in
21 solutions at pH = 3, 4, and 10. Substance (a) containing the 1,3-dioxane fragment in its structure
22 undergoes hydrolysis under the action of acid catalysts. In this case, the electron-donating
23 substituents in position 2 accelerate the rate of hydrolysis (Fig. 19). Thus, the 1,3-dioxane moiety
24 can undergo hydrolysis to form *tris*(hydroxymethyl)aminomethane (b) according to Fig. 19 [48].

25 It was found by NMR spectroscopy that at pH 3 and 4, the disappearance of the signals
26 is observed from the protons of the CH₃-groups (1.41–1.42 ppm), as well as the shift of the
27 chemical shifts of the CH₂-protons of aziridine rings in a strong field (from 2.33 to 2.16 and 2.07

1 ppm, respectively). These changes may indicate the hydrolysis of the 1,3-dioxane fragment with
2 the formation of the *tris*(hydroxymethyl)aminomethane derivative (b) at pH 3 and 4 (Fig. 20). The
3 formation of product (b) was also confirmed by mass spectrometry.

4 It was found by NMR spectroscopy that no noticeable shift of signals occurs in an
5 alkaline medium at pH = 10. Thus, it can be concluded that the structure of substance (a) is stable
6 in an alkaline medium (Fig. 21).

7 **3.5. Distribution in the octan-1-ol–H₂O system**

8 The substance (a) distribution coefficient between phases was calculated using Eq. 20:

$$9 \quad P_{ow} = \frac{c_o'}{c_w'} = \frac{c_w - c_w'}{c_w'}, \quad (20)$$

10 where c_o' and c_w' are the concentrations of substance (a) in octan-1-ol and water, respectively,
11 after distribution, c_w is the initial concentration of substance (a) in water.

12 The obtained value for substance (a) turned out to be $\lg P_{ow} = 0.16 \pm 0.01$. The indicated
13 value shows that substance (a) has practically the same affinity for the aqueous and lipid phases.
14 The literature data contain only one calculated value for the octan-1-ol–water partition coefficient
15 of substance (a): $\lg P_{ow} = 0.1$ [49]. This value was obtained using the XLOGP3-AA method [50].
16 XLOGP3-AA is an atom-additive method that calculates $\lg P_{ow}$ by adding up contributions from
17 each atom in the given molecule.

18 **3.6. Membrane mitochondrial potential**

19 As known from the literature, the mechanism of the cytotoxic action of doxorubicin is to
20 inhibit the activity of topoisomerase II, which leads to inhibiting DNA replication and damage to
21 mitochondria due to the inhibition of complex I of the electron donor chain and the decrease in the
22 mitochondrial potential [51]. The combination of these factors causes mitochondrial damage and
23 activation of oxidative stress.

24 The study showed that doxorubicin reduces the mitochondrial membrane potential by $45 \pm$
25 5% compared to the control. In the case of substance (a) no statistically significant effect on the
26 value of the mitochondrial membrane potential was observed. Thus, based on the results of

1 previous studies [1], we can conclude that the key mechanism of the cytostatic action of substance
2 (a) is the damaging effect on the DNA molecule.

3 **3.7. Electronic structure and Molecular Dynamics**

4 The results of calculating charges (average values for each type of atoms) for various
5 functionals and environments are given in Table 5. An increase in the dielectric constant of the
6 medium leads to an increase in the absolute values of the charges on the atoms. In this case, the
7 highest negative values belong to the oxygen atoms of the molecule. This means that the
8 interaction with polar solvents, in particular, solvation and hydrolysis will mainly be carried out
9 *via* carbon-oxygen bonds.

10 Molecular dynamics calculations have confirmed this approach. Table 6 shows the maxima
11 of the radial distribution functions (RDF) between water molecules and the corresponding atoms
12 of substance (a) (for designation, see Fig. 22). The closest approach of water molecules to oxygen
13 atoms of substance (a) increases the higher probability of breakage of carbon-oxygen bonds due
14 to the hydrolysis.

15 **3.8. Cytotoxicity**

16 The study of the cytotoxicity of substance (a) in relation to the cell lines Capan-2 (Fig. 23)
17 and SK-MEL-1 (Fig. 24) shows dose-dependent decrease in cell survival in the concentration
18 range $C = 0.098\text{--}50\ \mu\text{M}$. Fig. 25 summarises the data on the cytotoxicity of substance (a) on
19 various cell lines in comparison with such widely used cytotoxic drugs as doxorubicin and
20 cisplatin. It can be seen that substance (a) has the most pronounced effect towards the A549 cell
21 line (human adenocarcinomic cells), superior to that of doxorubicin and cisplatin. In the case of
22 other cell lines, the effect of substance (a) is comparable to that of cisplatin and is inferior in
23 effectiveness to doxorubicin. Separately, it should be noted that substance (a) has the lowest
24 cytotoxicity towards healthy HEK293 cells (human embryonic kidney cells) in comparison with
25 doxorubicin and cisplatin. The observed effect indicates a lower cytotoxicity of substance (a).

1 **3.9. Ehrlich ascites carcinoma murine model**

2 By the 8th day after tumour transplantation, the ascites was observed in all control mice and
3 was completely absent in the animals that received substance (a). Only by the 18th day the ascites
4 was observed in all mice of the substance (a) group (Table 7).

5 The lag in the accumulation of ascites under the influence of substance (a) was reflected in
6 the body weight of the animals. By the 12th day after the tumour transplantation, while the body
7 weight of the control mice increased by 14 % ($p = 0.0259$), the body weight of the mice that
8 received substance (a) did not differ from the initial weight, and only by the 16th day an increase
9 in the body weight was recorded (Table 8). The delay in tumour development under the influence
10 of substance (a) resulted in increased life expectancy of the animals (Fig. 26).

11 By the 24th day after transplantation, when 100 % of the control mice died, 80 % of the
12 animals in the group of mice injected with substance (a) remained alive ($p = 0.0003$). As a result
13 of substance (a) treatment, the risk of death from the tumour decreased by 69 % (HR 0.3099; 95
14 % CI 0.1105–0.8691; $p = 0.0006$). The life expectancy median for the mice that received substance
15 (a) increased by 42 % in comparison with the control group (Table 9).

16 The obtained results suggest the presence of a contact antitumor effect of substance (a).
17 This property allows to consider its use as promising treatment in other approaches of local
18 chemotherapy, including hyperthermic chemoperfusion of the abdominal cavity and intra-arterial
19 perfusion. The contact cytotoxicity of substance (a) can also be clinically used in intravesical
20 chemotherapy for superficial bladder cancer. Due to its amphiphilicity, substance (a) can be used
21 in oil solutions for chemoembolisation in patients with primary and metastatic liver cancer and in
22 kidney cancer.

23 **4. Conclusions**

24 We present novel experimental data on the physicochemical properties of substance (a)
25 aqueous solutions. It was revealed that the presence of substance (a) in aqueous solution leads to
26 solution structuring. It was shown that substance (a) is compatible with water and demonstrates
27 high stability in time in neutral and alkaline medium. The investigated distribution of substance

1 (a) between octan-1-ol and water has shown that its affinity is comparable for the aqueous and
2 lipid phases. A dose-dependent cytostatic effect of substance (a) was shown on Capan-2 and SK-
3 MEL-1 cell lines. The measurement of the mitochondrial membrane potential did not reveal the
4 effect of substance (a) on the functional activity of mitochondria. The therapeutic activity of
5 intraperitoneal administration of substance (a) in chemotherapy of abdominal carcinomatosis was
6 established in the model of Ehrlich ascites carcinoma. All results combined are of interest for
7 further medical applications of substance (a).

8 **Acknowledgements**

9 The work was supported by Russian Foundation for Basic Research (project number 21–
10 515–10007). The equipment of the following Resource Centres of the Research Park of Saint
11 Petersburg State University was used: Resource Centre ‘GeoModel’, the Centre for Diagnostics of
12 Functional Materials for Medicine, Pharmacology and Nanoelectronics, Interdisciplinary
13 Resource Centre for Nanotechnology, Magnetic Resonance Research Centre, Centre for Physical
14 Methods of Surface Investigation, Centre for Chemical Analysis and Materials Research,
15 Thermogravimetric and Calorimetric Research Centre.

16

1 **References**

- 2 [1] O. V Mikolaichuk, V. V Sharoyko, E.A. Popova, A. V Protas, A. V Fonin, L. V Vasina,
3 Y.A. Anufrikov, M.D. Luttsev, I.A. Nashchekina, A.M. Malkova, G. V Tochilnikov, S. V
4 Ageev, K.N. Semenov, Biocompatibility and bioactivity study of a cytostatic drug
5 belonging to the group of alkylating agents of the triazine derivative class, *J. Mol. Liq.* 343
6 (2021) 117630. [https://doi.org/https://doi.org/10.1016/j.molliq.2021.117630](https://doi.org/10.1016/j.molliq.2021.117630).
- 7 [2] V.B. Duong, P. Van Hien, T.T. Ngoc, P.D. Chau, T.K. Vu, A Simple synthesis of the
8 anticancer drug Altretamine, *Lett. Org. Chem.* 17 (2020) 628–630.
9 <https://doi.org/10.2174/1570178617666200210111041>.
- 10 [3] C. McIlwain, Triethylenemelamine, in: S.J. Enna, D.B.B.T.T.C.P.R. Bylund (Eds.),
11 XPharm Compr. Pharmacol. Ref., Elsevier, New York, 2008: pp. 1–4.
12 <https://doi.org/10.1016/B978-008055232-3.63946-7>.
- 13 [4] S.K. Vujjini, G. Varanasi, S. Arevelli, S.C. Kandala, S.R. Tirumalaraju, R. Bandichhor, M.
14 Kagga, P. Cherukupally, An Improved and scalable process for the synthesis of 5-
15 Azacytidine: an antineoplastic drug, *Org. Process Res. Dev.* 17 (2013) 303–306.
16 <https://doi.org/10.1021/op300192e>.
- 17 [5] J. Dubois, R. Arnould, F. Abikhalil, M. Hanocq, G. Atassi, G. Ghanem, A. Libert, F.J.
18 Lejeune, *In vitro* cytotoxicity of hexamethylmelamine (HMM) and its derivatives,
19 *Anticancer Res.* 10 (1990) 827–832. <http://www.ncbi.nlm.nih.gov/pubmed/2114821>.
- 20 [6] G. Jack, L. Doyle, M.M. Palejwalla, Tretamine in the treatment of inoperable lung cancer,
21 *Lancet.* 275 (1960) 206–207. [https://doi.org/10.1016/S0140-6736\(60\)90118-5](https://doi.org/10.1016/S0140-6736(60)90118-5).
- 22 [7] T. Kiziltepe, T. Hideshima, L. Catley, N. Raje, H. Yasui, N. Shiraishi, Y. Okawa, H. Ikeda,
23 S. Vallet, S. Pozzi, K. Ishitsuka, E.M. Ocio, D. Chauhan, K.C. Anderson, 5-Azacytidine, a
24 DNA methyltransferase inhibitor, induces ATR-mediated DNA double-strand break
25 responses, apoptosis, and synergistic cytotoxicity with doxorubicin and bortezomib against
26 multiple myeloma cells, *Mol. Cancer Ther.* 6 (2007) 1718–1727.
27 <https://doi.org/10.1158/1535-7163.MCT-07-0010>.

- 1 [8] P. Singla, V. Luxami, K. Paul, Triazine as a promising scaffold for its versatile biological
2 behavior, *Eur. J. Med. Chem.* 102 (2015) 39–57.
3 <https://doi.org/10.1016/j.ejmech.2015.07.037>.
- 4 [9] V.G. Bespalov, E.A. Vyshinskaya, I.N. Vasil'eva, A.L. Semenov, M.A. Maidin, N. V
5 Barakova, A.N. Stukov, Comparative study of antitumor efficiency of intraperitoneal and
6 intravenous cytostatics in experimental rats with disseminated ovarian cancer, *Bull. Exp.*
7 *Biol. Med.* 162 (2017) 383–386. <https://doi.org/10.1007/s10517-017-3621-5>.
- 8 [10] A.E. Borisov, M.L. Gershanovich, V.P. Zemlianoĭ, S.L. Nepomniashchaia, A.N. Stukov,
9 V.A. Filov, The use of dioxadet in chemoembolization of the hepatic artery in primary and
10 metastatic cancer of the liver, *Vopr. Onkol.* 44 (1998) 714–717.
11 <http://www.ncbi.nlm.nih.gov/pubmed/10087972>.
- 12 [11] V.G. Bespalov, A.A. Zhabin, A.N. Stukov, O.A. Beliaeva, Y.G. Murazov, A.L. Semenov,
13 S.A. Kon'kov, I.M. Krylova, Synergism of antitumor action of dioxadet and cisplatin in
14 model of ascitic ovarian tumor, *Sib. J. Oncol.* 1 (2013) 42–46.
15 <https://www.siboncoj.ru/jour/article/view/48/50>.
- 16 [12] V.A. Filov, A.N. Stukov, L.L. Malyugina, B.A. Ivin, Study of antitumor activity and
17 toxicity of Dioxadet, *Experimental Oncol.* 18 (1996) 84–86.
- 18 [13] V.G. Bespalov, G.S. Kireeva, O.A. Belyaeva, O.E. Kalinin, K.Y. Senchik, A.N. Stukov,
19 G.I. Gafton, K.D. Guseynov, A.M. Belyaev, Both heat and new chemotherapeutic drug
20 dioxadet in hyperthermic intraperitoneal chemoperfusion improved survival in rat ovarian
21 cancer model, *J. Surg. Oncol.* 113 (2016) 438–442. <https://doi.org/10.1002/jso.24140>.
- 22 [14] D.K. Latipova, M.L. Gershanovich, A.N. Stukov, T.I. Semiglazova, L. V Filatova, A.A.
23 Tarasenkova, S.F. Vershinina, S.A. Kon'kov, I.M. Krylova, V.G. Bespalov, A. V
24 Panchenko, I.G. Murazov, Synergism of antitumor activity of gemcitabine and dioxadet in
25 mice with ascitic Ehrlich's tumor, *Vopr. Onkol.* 57 (2011) 767–70.
26 <http://www.ncbi.nlm.nih.gov/pubmed/22416395>.
- 27 [15] G. Patrick, *An Introduction to Medicinal Chemistry*, Oxford University Press, 2017.

- 1 [https://global.oup.com/academic/product/an-introduction-to-medicinal-chemistry-](https://global.oup.com/academic/product/an-introduction-to-medicinal-chemistry-9780198749691?q=An+Introduction+to+Medicinal+Chemistry&lang=en&cc=ru)
2 [9780198749691?q=An Introduction to Medicinal Chemistry&lang=en&cc=ru.](https://global.oup.com/academic/product/an-introduction-to-medicinal-chemistry-9780198749691?q=An+Introduction+to+Medicinal+Chemistry&lang=en&cc=ru)
- 3 [16] W. Czechtizky, P. Hamley, Small molecule medicinal chemistry: strategies and
4 technologies, Wiley, 2015. [https://www.wiley.com/en-](https://www.wiley.com/en-au/Small+Molecule+Medicinal+Chemistry%3A+Strategies+and+Technologies-p-9781118771600)
5 [au/Small+Molecule+Medicinal+Chemistry%3A+Strategies+and+Technologies-p-](https://www.wiley.com/en-au/Small+Molecule+Medicinal+Chemistry%3A+Strategies+and+Technologies-p-9781118771600)
6 [9781118771600.](https://www.wiley.com/en-au/Small+Molecule+Medicinal+Chemistry%3A+Strategies+and+Technologies-p-9781118771600)
- 7 [17] R.B. Silverman, M.W. Holladay, The Organic Chemistry of Drug Design and Drug Action:
8 Third Edition, Elsevier Inc., 2015. [https://doi.org/10.1016/C2009-0-64537-2.](https://doi.org/10.1016/C2009-0-64537-2)
- 9 [18] A. V. Kustov, O.A. Antonova, N.L. Smirnova, A.A. Kladiev, A.A. Kladiev, T. V.
10 Kudayarova, M.S. Gruzdev, D.B. Berezin, The energetics of solvation and ion-ion
11 interactions in prospidium chloride aqueous solutions, J. Mol. Liq. 263 (2018) 49–52.
12 [https://doi.org/10.1016/j.molliq.2018.04.118.](https://doi.org/10.1016/j.molliq.2018.04.118)
- 13 [19] H. Akbaş, A. Karadağ, A. Aydın, A. Destegül, Z. Kılıç, Synthesis, structural and thermal
14 properties of the hexapyrrolidinocyclotriphosphazenes-based protic molten salts:
15 Antiproliferative effects against HT29, HeLa, and C6 cancer cell lines, J. Mol. Liq. 230
16 (2017) 482–495. [https://doi.org/10.1016/j.molliq.2017.01.067.](https://doi.org/10.1016/j.molliq.2017.01.067)
- 17 [20] T.Y. Nikolaienko, Interaction of anticancer drug doxorubicin with sodium oleate bilayer:
18 Insights from molecular dynamics simulations, J. Mol. Liq. 235 (2017) 31–43.
19 [https://doi.org/10.1016/j.molliq.2016.11.065.](https://doi.org/10.1016/j.molliq.2016.11.065)
- 20 [21] A. Jouyban, E. Rahimpour, Z. Karimzadeh, A new correlative model to simulate the
21 solubility of drugs in mono-solvent systems at various temperatures, J. Mol. Liq. 343 (2021)
22 117587. [https://doi.org/10.1016/j.molliq.2021.117587.](https://doi.org/10.1016/j.molliq.2021.117587)
- 23 [22] J. Gurung, J. Anjudikkal, A.K. Pulikkal, Amphiphilic drug–additive systems in aqueous and
24 organic solvent–water mixed media: A comprehensive account on physicochemical
25 properties, J. Mol. Liq. 318 (2020) 114221. [https://doi.org/10.1016/j.molliq.2020.114221.](https://doi.org/10.1016/j.molliq.2020.114221)
- 26 [23] M. Mondal, S. Basak, S. Choudhury, N.N. Ghosh, M.N. Roy, Investigation of molecular
27 interactions insight into some biologically active amino acids and aqueous solutions of an

- 1 anti-malarial drug by physicochemical and theoretical approach, *J. Mol. Liq.* 341 (2021)
2 116933. <https://doi.org/10.1016/j.molliq.2021.116933>.
- 3 [24] F.A. Alhumaydhi, M.A. Aljasir, A.S.M. Aljohani, S.A. Alsagaby, A.S.S. Alwashmi, M.
4 Shahwan, M.I. Hassan, A. Islam, A. Shamsi, Probing the interaction of memantine, an
5 important Alzheimer's drug, with human serum albumin: *In silico* and *in vitro* approach, *J.*
6 *Mol. Liq.* 340 (2021) 116888. <https://doi.org/10.1016/j.molliq.2021.116888>.
- 7 [25] G.M. Sheldrick, SHELXT – Integrated space-group and crystal-structure determination,
8 *Acta Crystallogr. Sect. A Found. Adv.* 71 (2015) 3–8.
9 <https://doi.org/10.1107/S2053273314026370>.
- 10 [26] G.M. Sheldrick, Crystal structure refinement with SHELXL, *Acta Crystallogr. Sect. C*
11 *Struct. Chem.* 71 (2015) 3–8. <https://doi.org/10.1107/S2053229614024218>.
- 12 [27] O. V Dolomanov, L.J. Bourhis, R.J. Gildea, J.A.K. Howard, H. Puschmann, OLEX2 : a
13 complete structure solution, refinement and analysis program, *J. Appl. Crystallogr.* 42
14 (2009) 339–341. <https://doi.org/10.1107/S0021889808042726>.
- 15 [28] V. V. Sharoyko, S. V. Ageev, A.A. Meshcheriakov, A. V. Akentiev, B.A. Noskov, I.T.
16 Rakipov, N.A. Charykov, N.A. Kulenova, B.K. Shaimardanova, N.E. Podolsky, K.N.
17 Semenov, Physicochemical study of water-soluble C₆₀(OH)₂₄ fulleranol, *J. Mol. Liq.* 311
18 (2020) 113360. <https://doi.org/10.1016/j.molliq.2020.113360>.
- 19 [29] E.I. Pochkaeva, A.A. Meshcheriakov, S. V. Ageev, N.E. Podolsky, A. V. Petrov, N.A.
20 Charykov, L. V. Vasina, O.Y. Nikolaeva, I.N. Gaponenko, V. V. Sharoyko, I. V. Murin,
21 K.N. Semenov, Polythermal density and viscosity, nanoparticle size distribution, binding
22 with human serum albumin and radical scavenging activity of the C₆₀-L-arginine
23 (C₆₀(C₆H₁₃N₄O₂)₈H₈) aqueous solutions, *J. Mol. Liq.* 297 (2020) 111915.
24 <https://doi.org/10.1016/j.molliq.2019.111915>.
- 25 [30] S. V. Ageev, G.O. Iurev, N.E. Podolsky, I.T. Rakipov, L. V. Vasina, B.A. Noskov, A. V.
26 Akentiev, N.A. Charykov, I. V. Murin, K.N. Semenov, Density, speed of sound, viscosity,
27 refractive index, surface tension and solubility of C₆₀[C(COOH)₂]₃, *J. Mol. Liq.* 291 (2019)

- 1 111256. <https://doi.org/10.1016/j.molliq.2019.111256>.
- 2 [31] E.B. Serebryakov, D.N. Zakusilo, K.N. Semenov, N.A. Charykov, A. V. Akentiev, B.A.
3 Noskov, A. V. Petrov, N.E. Podolsky, A.S. Mazur, L. V. Dul'neva, I. V. Murin, Physico-
4 chemical properties of C₇₀-L-threonine bisadduct (C₇₀(C₄H₉NO₂)₂) aqueous solutions, J.
5 Mol. Liq. 279 (2019) 687–699. <https://doi.org/10.1016/j.molliq.2019.02.013>.
- 6 [32] N.E. Podolsky, M.A. Marcos, D. Cabaleiro, K.N. Semenov, L. Lugo, A. V. Petrov, N.A.
7 Charykov, V. V. Sharoyko, T.D. Vlasov, I. V. Murin, Physico-chemical properties of
8 C₆₀(OH)_{22–24} water solutions: Density, viscosity, refraction index, isobaric heat capacity and
9 antioxidant activity, J. Mol. Liq. 278 (2019) 342–355.
10 <https://doi.org/10.1016/j.molliq.2018.12.148>.
- 11 [33] E.B. Serebryakov, K.N. Semenov, I. V. Stepanyuk, N.A. Charykov, A.N. Mescheryakov,
12 A.N. Zhukov, A. V. Chaplygin, I. V. Murin, Physico-chemical properties of the C₇₀-L-lysine
13 aqueous solutions, J. Mol. Liq. 256 (2018) 507–518.
14 <https://doi.org/10.1016/j.molliq.2018.02.057>.
- 15 [34] K.N. Semenov, N.A. Charykov, A.A. Meshcheriakov, E. Lahderanta, A. V. Chaplygin,
16 Y.A. Anufrikov, I. V. Murin, Physico-chemical properties of the C₆₀-L-threonine water
17 solutions, J. Mol. Liq. 242 (2017) 940–950. <https://doi.org/10.1016/j.molliq.2017.07.098>.
- 18 [35] K.N. Semenov, N.A. Charykov, G.O. Iurev, N.M. Ivanova, V.A. Keskinov, D.G. Letenko,
19 V.N. Postnov, V. V. Sharoyko, N.A. Kulenova, I. V. Prikhodko, I. V. Murin, Physico-
20 chemical properties of the C₆₀-L-lysine water solutions, J. Mol. Liq. 225 (2017) 767–777.
21 <https://doi.org/10.1016/j.molliq.2016.11.003>.
- 22 [36] O.S. Manyakina, K.N. Semenov, N.A. Charykov, N.M. Ivanova, V.A. Keskinov, V. V.
23 Sharoyko, D.G. Letenko, V.A. Nikitin, V. V. Klepikov, I. V. Murin, Physico-chemical
24 properties of the water-soluble C₇₀-tris-malonic solutions, J. Mol. Liq. 211 (2015) 487–493.
25 <https://doi.org/10.1016/j.molliq.2015.06.071>.
- 26 [37] A.A. Shestopalova, K.N. Semenov, N.A. Charykov, V.N. Postnov, N.M. Ivanova, V. V.
27 Sharoyko, V.A. Keskinov, D.G. Letenko, V.A. Nikitin, V. V. Klepikov, I. V. Murin,

- 1 Physico-chemical properties of the C₆₀-arginine water solutions, *J. Mol. Liq.* 211 (2015)
2 301–307. <https://doi.org/10.1016/j.molliq.2015.07.022>.
- 3 [38] K.N. Semenov, N.A. Charykov, I. V. Murin, Y. V. Pukharenko, Physico-chemical
4 properties of the C₆₀-tris-malonic derivative water solutions, *J. Mol. Liq.* 201 (2015) 50–
5 58. <https://doi.org/10.1016/j.molliq.2014.11.019>.
- 6 [39] K.N. Semenov, N.A. Charykov, I. V. Murin, Y. V. Pukharenko, Physico-chemical
7 properties of the fullereneol-70 water solutions, *J. Mol. Liq.* 202 (2015) 1–8.
8 <https://doi.org/10.1016/j.molliq.2014.12.002>.
- 9 [40] V. V. Sharoyko, S. V. Ageev, A.A. Meshcheriakov, N.E. Podolsky, J.P. Vallejo, L. Lugo,
10 I.T. Rakipov, A. V. Petrov, A. V. Ivanova, N.A. Charykov, K.N. Semenov,
11 Physicochemical investigation of water-soluble C₆₀(C₂NH₄O₂)₄H₄ (C₆₀-Gly) adduct, *J. Mol.*
12 *Liq.* 344 (2021) 117658. <https://doi.org/10.1016/j.molliq.2021.117658>.
- 13 [41] A.O.E. Abdelhalim, V. V. Sharoyko, A.A. Meshcheriakov, S.D. Martynova, S. V. Ageev,
14 G.O. Iurev, H. Al Mulla, A. V. Petrov, I.L. Solovtsova, L. V. Vasina, I. V. Murin, K.N.
15 Semenov, Reduction and functionalization of graphene oxide with L-cysteine: Synthesis,
16 characterization and biocompatibility, *Nanomedicine Nanotechnology, Biol. Med.* 29
17 (2020) 102284. <https://doi.org/10.1016/j.nano.2020.102284>.
- 18 [42] M.J. Blandamer, M.I. Davis, G. Douhéret, J.C.R. Reis, Apparent molar isentropic
19 compressions and expansions of solutions, *Chem. Soc. Rev.* 30 (2001) 8–15.
20 <https://doi.org/10.1039/a908547e>.
- 21 [43] S. Ebrahimi, R. Sadeghi, Density, speed of sound, and viscosity of some binary and ternary
22 aqueous polymer solutions at different temperatures, *J. Chem. Eng. Data.* 60 (2015) 3132–
23 3147. <https://doi.org/10.1021/acs.jced.5b00290>.
- 24 [44] L. Šimurka, I. Cibulka, L. Hnědkovský, Partial molar isentropic compressions and partial
25 molar volumes of selected branched aliphatic alcohols at infinite dilution in water at
26 temperatures from $T = (278 \text{ to } 318) \text{ K}$ and atmospheric pressure, *J. Chem. Eng. Data.* 57
27 (2012) 1570–1580. <https://doi.org/10.1021/je300175w>.

- 1 [45] M.S. Alam, B. Ashokkumar, A. Mohammed Siddiq, The density, dynamic viscosity and
2 kinematic viscosity of protic polar solvents (pure and mixed systems) studies: A theoretical
3 insight of thermophysical properties, *J. Mol. Liq.* 251 (2018) 458–469.
4 <https://doi.org/10.1016/j.molliq.2017.12.089>.
- 5 [46] L.S. Garca-Coln, L.F. del Castillo, P. Goldstein, Theoretical basis for the Vogel-Fulcher-
6 Tammann equation, *Phys. Rev. B.* 40 (1989) 7040–7044.
7 <https://doi.org/10.1103/PhysRevB.40.7040>.
- 8 [47] B. V Ioffe, Refractometry as a method for the physicochemical analysis of organic systems,
9 *Russ. Chem. Rev.* 29 (1960) 53–66. <https://doi.org/10.1070/rc1960v029n02abeh001218>.
- 10 [48] I. Apok, M. Bartok, R.A. Karakhanov, N.I. Shuikin, Chemical properties of 1,3-dioxans,
11 *Russ. Chem. Rev.* 38 (1969) 72–92.
12 <https://doi.org/10.1070/RC1969v038n01ABEH001723>.
- 13 [49] Dioxadet | $C_{14}H_{22}N_6O_3$ - PubChem, (n.d.).
14 <https://pubchem.ncbi.nlm.nih.gov/compound/48858>.
- 15 [50] C. Tiejun, Z. Yuan, L. Xun, L. Fu, X. Yong, Z. Xinglong, L. Yan, R. Wang, L. Lai,
16 Computation of octanol–water partition coefficients by guiding an additive model with
17 knowledge, *J. Chem. Inf. Model.* 47 (2007) 2140–2148.
18 <https://doi.org/10.1021/CI700257Y>.
- 19 [51] Y. Pommier, E. Leo, H. Zhang, C. Marchand, DNA Topoisomerases and Their Poisoning
20 by Anticancer and Antibacterial Drugs, *Chem. Biol.* 17 (2010) 421–433.
21 <https://doi.org/10.1016/j.chembiol.2010.04.012>.
- 22 [52] O. Akiyode, D. George, G. Getti, J. Boateng, Systematic comparison of the functional
23 physico-chemical characteristics and biocidal activity of microbial derived biosurfactants
24 on blood-derived and breast cancer cells, *J. Colloid Interface Sci.* 479 (2016) 221–233.
25 <https://doi.org/10.1016/j.jcis.2016.06.051>.
- 26 [53] A. Amuthan, V. Devi, C.S. Shreedhara, V. Rao, R. Lobo, Cytoprotective Activity of
27 Neichitti (*Vernonia cinerea*) in Human Embryonic Kidney (HEK293) Normal Cells and

- 1 Human Cervix Epitheloid Carcinoma (HeLa) Cells against Cisplatin Induced Toxicity: A
2 Comparative Study, J. Clin. Diagnostic Res. 13 (2019) KC01–KC06.
3 <https://doi.org/10.7860/JCDR/2019/40242.12624>.
- 4 [54] Z. Farhane, F. Bonnier, O. Howe, A. Casey, H.J. Byrne, Doxorubicin kinetics and effects
5 on lung cancer cell lines using *in vitro* Raman micro-spectroscopy: binding signatures, drug
6 resistance and DNA repair, J. Biophotonics. 11 (2018) e201700060.
7 <https://doi.org/10.1002/jbio.201700060>.
- 8 [55] Drug: Cisplatin - Cancerrxgene - Genomics of Drug Sensitivity in Cancer, (n.d.).
9 <https://www.cancerrxgene.org/compound/Cisplatin/1005/by-tissue?>
- 10 [56] Drug: Doxorubicin - Cancerrxgene - Genomics of Drug Sensitivity in Cancer, (n.d.).
11 <https://www.cancerrxgene.org/compound/Doxorubicin/133/by-tissue?>
- 12 [57] K. Gorshkov, N. Sima, W. Sun, B. Lu, W. Huang, J. Travers, C. Klumpp-Thomas, S.G.
13 Michael, T. Xu, R. Huang, E.M. Lee, X. Cheng, W. Zheng, Quantitative chemotherapeutic
14 profiling of gynecologic cancer cell lines using approved drugs and bioactive compounds,
15 Transl. Oncol. 12 (2019) 441–452. <https://doi.org/10.1016/j.tranon.2018.11.016>.
- 16 [58] S. Zheng, X. Wang, Y.-H. Weng, X. Jin, J.-L. Ji, L. Guo, B. Hu, N. Liu, Q. Cheng, J. Zhang,
17 H. Bai, T. Yang, X.-H. Xia, H.-Y. Zhang, S. Gao, Y. Huang, siRNA Knockdown of RRM2
18 effectively suppressed pancreatic tumor growth alone or synergistically with doxorubicin,
19 Mol. Ther. - Nucleic Acids. 12 (2018) 805–816.
20 <https://doi.org/10.1016/j.omtn.2018.08.003>.
- 21 [59] M. Beer, N. Kuppalu, M. Stefanini, H. Becker, I. Schulz, S. Manoli, J. Schuette, C.
22 Schmees, A. Casazza, M. Stelzle, A. Arcangeli, A novel microfluidic 3D platform for
23 culturing pancreatic ductal adenocarcinoma cells: comparison with *in vitro* cultures and *in*
24 *vivo* xenografts, Sci. Rep. 7 (2017) 1–12. <https://doi.org/10.1038/s41598-017-01256-8>.
- 25 [60] J.-C. Hahm, I.-K. Lee, W.-K. Kang, S.-U. Kim, Y.-J. Ahn, Cytotoxicity of neolignans
26 identified in *Saururus chinensis* towards human cancer cell lines, Planta Med. 71 (2005)
27 464–469. <https://doi.org/10.1055/S-2005-864143>.

1 Table 1. Viscous flow activation parameters for substance (a) aqueous solutions.

$C / \text{g}\cdot\text{dm}^{-3}$	$E_a / \text{J}\cdot\text{mol}^{-1}$	$\ln A_s / \ln[\text{mPa}\cdot\text{s}]$	T_A / K	$\Delta H / \text{kJ}\cdot\text{mol}^{-1}$	$\Delta S / \text{J}\cdot\text{mol}^{-1}$
0.025	15118.67	-6.21	292.94	14.81	-5.09
0.10	15099.15	-6.20	292.88	14.79	-5.15
0.25	15115.69	-6.21	292.94	14.81	-5.10
0.55	15108.14	-6.20	292.94	14.80	-5.13
1.0	15052.56	-6.18	293.04	14.75	-5.33
2.5	15124.00	-6.20	293.22	14.82	-5.12
5.0	15187.55	-6.22	293.87	14.88	-5.01
10	15091.71	-6.15	295.35	14.77	-5.62

2

1 Table 2. Correlation parameters for the VFT equation ($\lg \eta(T) = \lg \eta_0 + \frac{A}{T-B}$).

Parameter	$C / \text{g}\cdot\text{dm}^{-3}$							
	0.025	0.1	0.25	0.55	1	2.5	5	10
$\lg \eta_0 / \lg[\text{mPa}\cdot\text{s}]$	-1.3096	-1.3241	-1.3032	-1.3321	-1.3267	-1.3254	-1.3295	-1.2895
A / K	160.8	165.1	159.0	167.4	166.9	165.9	168.0	161.6
B / K	170.8	168.8	171.5	167.9	167.8	168.6	168.0	170.4
$\text{SD} / \text{mPa}\cdot\text{s}$	0.00048	0.00032	0.00062	0.00039	0.00071	0.00064	0.00026	0.00277
$\text{AAD} / \%$	0.17	0.12	0.12	0.12	0.12	0.03	0.07	0.23

2

Table 3. Refraction properties of substance (a) aqueous solutions at 293.15 K.

$w / \%$	$x \cdot 10^3$	n_D	$r / \text{cm}^3 \cdot \text{g}^{-1}$	$R / \text{cm}^3 \cdot \text{mol}^{-1}$	$r_a / \text{cm}^3 \cdot \text{g}^{-1}$	$R_a / \text{cm}^3 \cdot \text{mol}^{-1}$
0.0025	0.0014	1.3330	0.2060	3.7088	—	—
0.010	0.0056	1.3330	0.2060	3.7091	—	—
0.025	0.014	1.3330	0.2061	3.7096	—	—
0.050	0.031	1.3331	0.2061	3.7106	—	—
0.10	0.056	1.3331	0.2061	3.7122	—	—
0.25	0.14	1.3332	0.2062	3.7175	0.4451	127.46
0.50	0.28	1.3338	0.2062	3.7264	0.3257	96.85
1.00	0.57	1.3345	0.2064	3.7442	0.2862	81.54
1.50	0.85	1.3353	0.2066	3.7622	0.2748	76.47
2.50	1.44	1.3369	0.2070	3.7991	0.2649	72.45

Table 4. Fitting parameters a , b_i , c_j ($i, j = 1-4$) for T - C dependences of density (ρ), speed of sound (u), viscosity (η), and refraction indices (n_D) of substance (a) aqueous solutions according to Eq. 19. R^2 is the coefficient of determination.

Solution	a	b_1	b_2	b_3	b_4	c_1	c_2	c_3	c_4	R^2
property										
$\rho / \text{g}\cdot\text{cm}^{-3}$	-5.12	0.076	$-3.53\cdot 10^{-4}$	$7.32\cdot 10^{-7}$	$-5.76\cdot 10^{-10}$	$3.70\cdot 10^{-4}$	$-1.57\cdot 10^{-4}$	$4.26\cdot 10^{-5}$	$-2.81\cdot 10^{-6}$	0.99967
$u / \text{m}\cdot\text{s}^{-1}$	-14072.04	161.83	-0.64	$1.15\cdot 10^{-3}$	$-8.00\cdot 10^{-7}$	0.48	0.11	-0.011	$2.75\cdot 10^{-4}$	0.99978
$\eta / \text{mPa}\cdot\text{s}$	507.88	-6.04	0.027	$-5.46\cdot 10^{-5}$	$4.13\cdot 10^{-8}$	$3.24\cdot 10^{-3}$	$-1.18\cdot 10^{-3}$	$3.07\cdot 10^{-4}$	$-1.84\cdot 10^{-5}$	0.99960
n_D	2.49	-0.016	$8.24\cdot 10^{-5}$	$-1.87\cdot 10^{-7}$	$1.56\cdot 10^{-10}$	$1.64\cdot 10^{-4}$	$-1.32\cdot 10^{-6}$	$1.04\cdot 10^{-7}$	$-2.03\cdot 10^{-9}$	0.99926

Table 5. Average charges on substance (a) atoms

Medium	ϵ	Carbon	Nitrogen	Hydrogen	Oxygen
<i>PBE</i>					
vacuum	1	0.276	-0.335	0.270	-0.476
<i>n</i> -hexane	1.89	0.281	-0.338	0.279	-0.485
acetonitrile	37.5	0.287	-0.342	0.294	-0.507
water	78.54	0.288	-0.342	0.294	-0.507
<i>PW91</i>					
vacuum	1	0.271	-0.334	0.270	-0.489
<i>n</i> -hexane	1.89	0.276	-0.337	0.213	-0.499
acetonitrile	37.5	0.282	-0.339	0.217	-0.519
water	78.54	0.283	-0.341	0.294	-0.520
<i>HCTH</i>					
vacuum	1	0.340	-0.373	0.257	-0.500
<i>n</i> -hexane	1.89	0.345	-0.377	0.204	-0.507
acetonitrile	37.5	0.348	-0.381	0.279	-0.527
water	78.54	0.352	-0.381	0.270	-0.527

Table 6. The values of the maxima of the RDF between substance (a) atoms and water (for designation, see Fig. 22).

Atom type	N4	N5	N6	N7	N8	N9	O1	O2	O3
RDF / Å	3.65	3.71	3.95	3.59	4.79	3.55	3.57	3.49	3.43

Table 7. Effect of substance (a) on the timing of ascites in BALB/c mice with Ehrlich carcinoma.

Days after transplantation	Number (%) of mice without ascites		<i>p</i>
	Control	Substance (a)	
8	0 (0 %)	10 (100 %)	$<10^{-4}$
10	0 (0 %)	10 (100 %)	$<10^{-4}$
12	0 (0 %)	10 (100 %)	$<10^{-4}$
14	0 (0 %)	9 (90 %)	10^{-4}
16	0 (0 %)	5 (50 %)	$9.8 \cdot 10^{-3}$
18	0 (0 %)	0 (0 %)	

Table 8. Effect of substance (a) on body weight change in BALB/c mice with Ehrlich ascites tumour.

Days after transplantation	Control ($n = 10$)		Substance (a) $5 \text{ mg}\cdot\text{kg}^{-1}$ ($n = 10$)	
	Body mass	% to the original	Body mass	% to the original
0	35.6 ± 0.8	100 %	35.3 ± 0.7	100 %
6	36.3 ± 1.1	102 %	33.9 ± 0.8	96 %
		$p = 0.5241$		$p = 0.1864$
8	39.2 ± 1.0	110 %	33.9 ± 1.0	96 %
		$p = 0.0112$		$p = 0.2302$
10	39.4 ± 1.0	111 %	34.6 ± 0.9	98 %
		$p = 0.0085$		$p = 0.4915$
12	40.6 ± 1.2	114 %	35.4 ± 0.7	100 %
		$p = 0.0033$		$p = 0.6827$
14	39.7 ± 1.5	112 %	35.5 ± 1.1	100 %
		$p = 0.0259$		$p = 0.8804$
16	40.2 ± 2.2	113 %	38.3 ± 1.3	113 %
		$p = 0.0541$		$p = 0.0121$

Table 9. Effect of substance (a) on the life expectancy median of mice with Ehrlich ascites carcinoma.

Group	Number of mice / alive over 60 days (% , <i>p</i>)	Life expectancy median (days)	75 % confidence interval	Increase in life expectancy	<i>p</i> (Mann– Whitney test)
Control	10/0	19.00	18.00–21.50	—	—
Substance (a)	10/0	27.00	23.75–30.25	42 %	0.0060

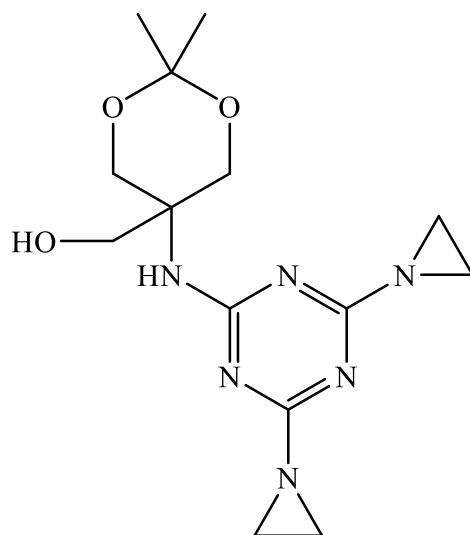


Fig. 1. The structure of substance (a).

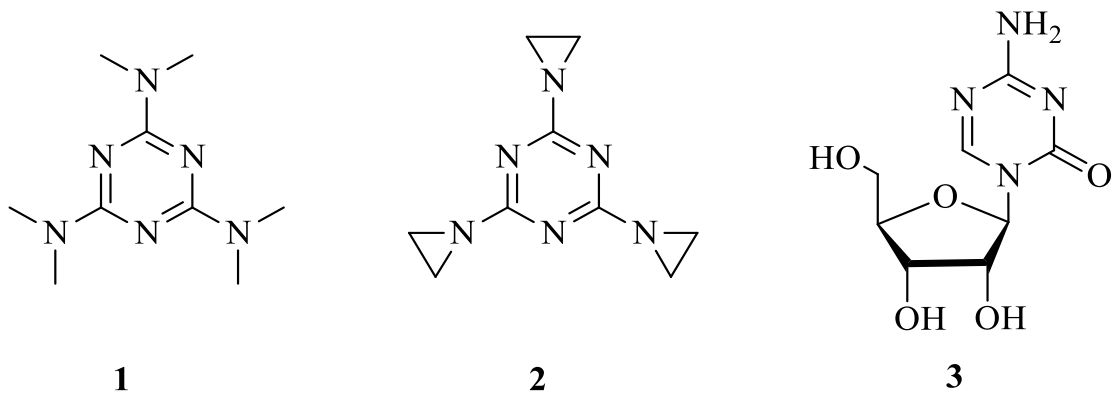


Fig. 2. The structures of anticancer drugs: Altretamine (1), Tretamine (2) and Azacitidine (3).

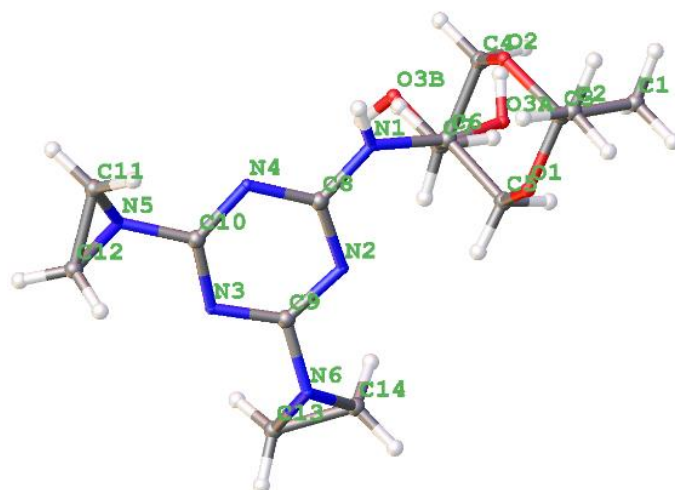


Fig. 3. Crystallographic data for substance (a) (CCDC 2074787).

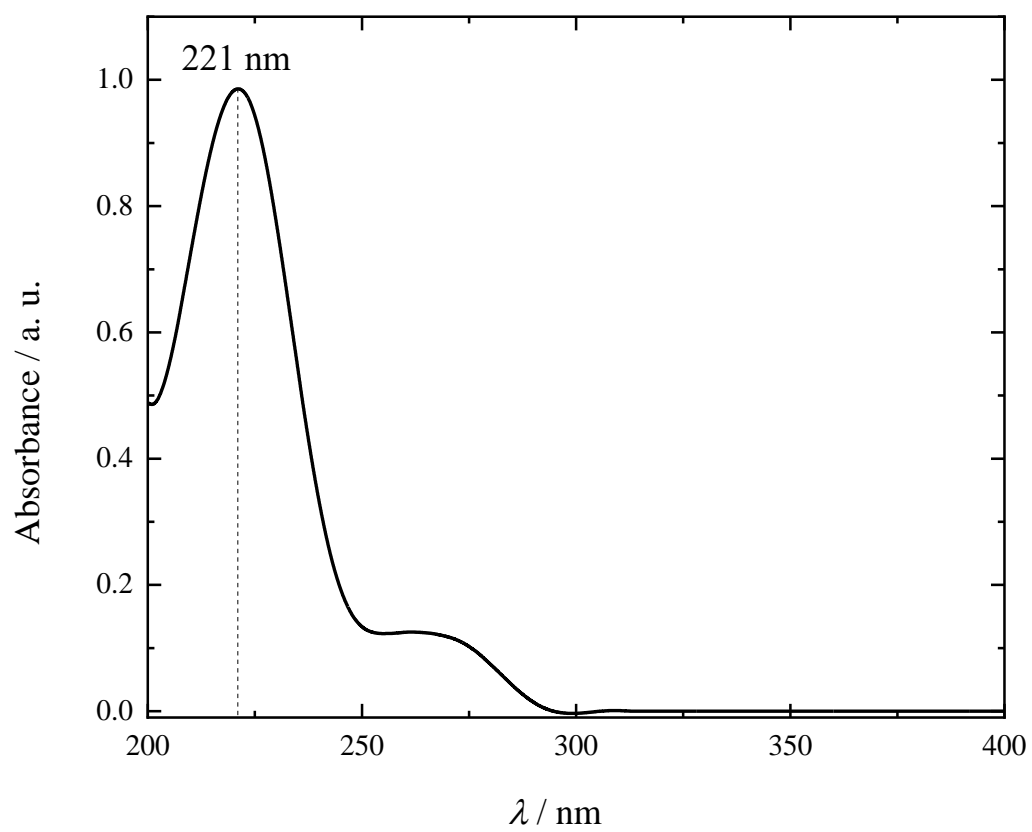


Fig. 4. The UV/Vis spectrum of substance (a) ($C = 0.055 \text{ g}\cdot\text{dm}^{-3}$) ($l = 1 \text{ cm}$).

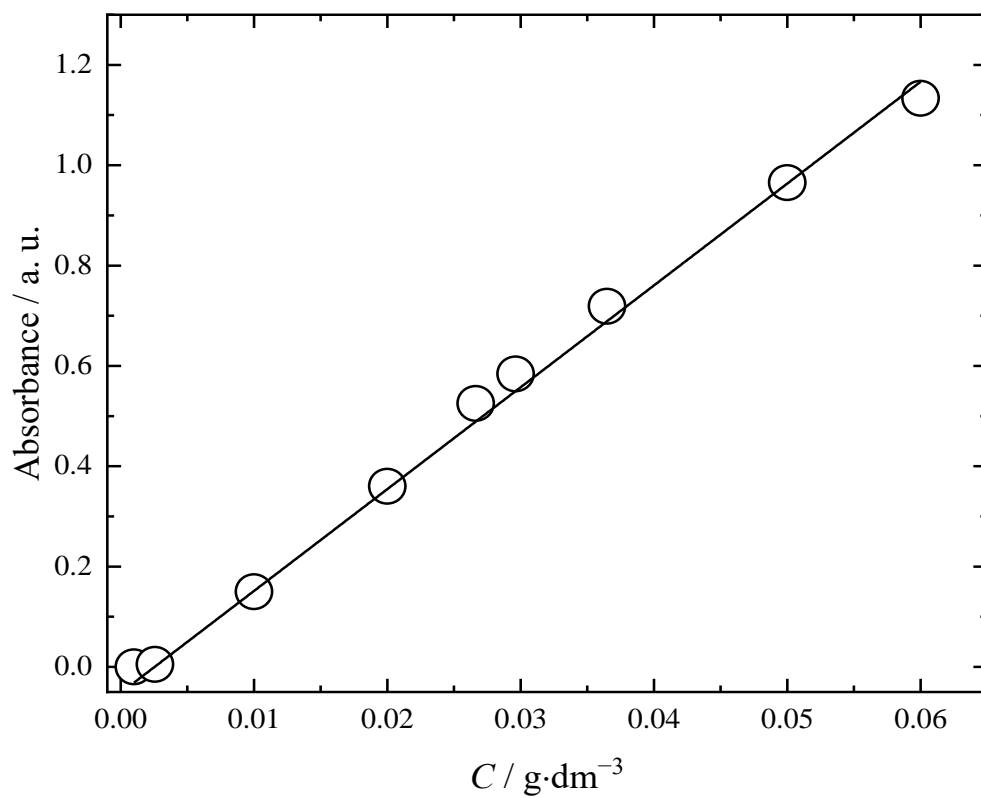


Fig. 5. Beer–Lambert–Bouguer law for substance (a) aqueous solutions ($R^2 = 0.989$) ($\lambda = 221 \text{ nm}$).

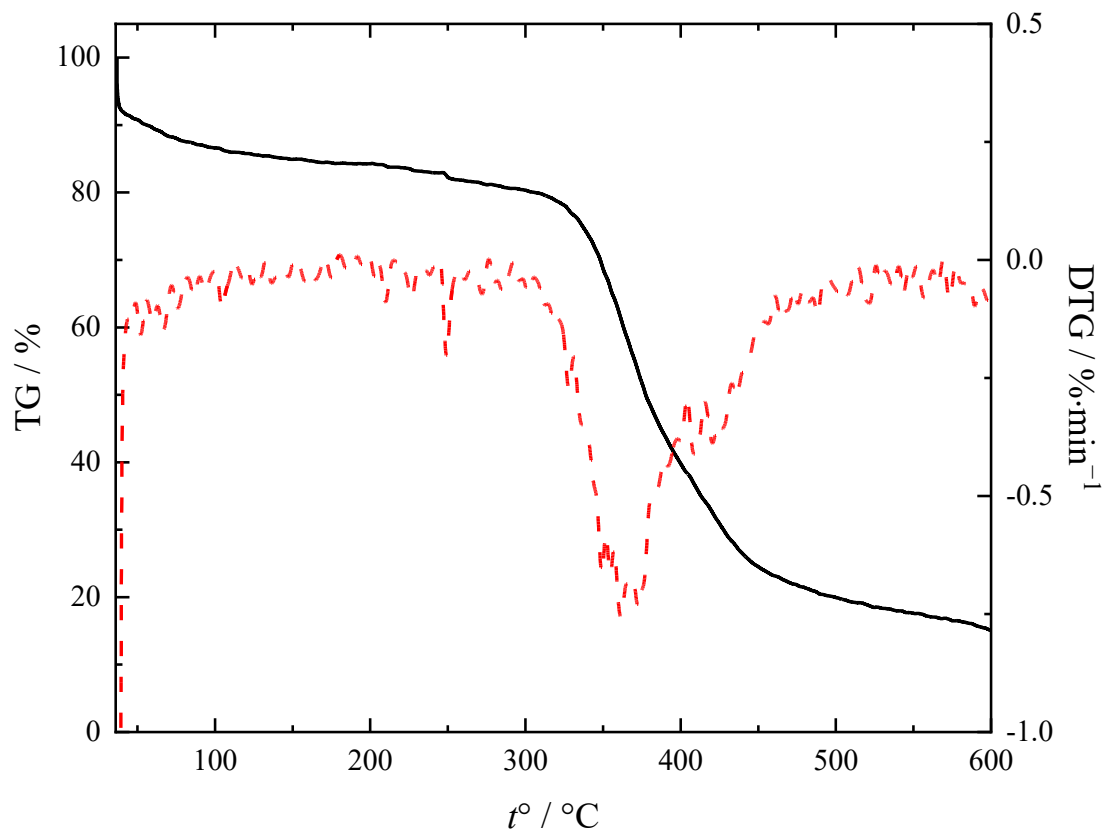


Fig. 6. TG (dashed line) and DTG (solid line) of substance (a) at $t^\circ = 40\text{--}600$ °C.

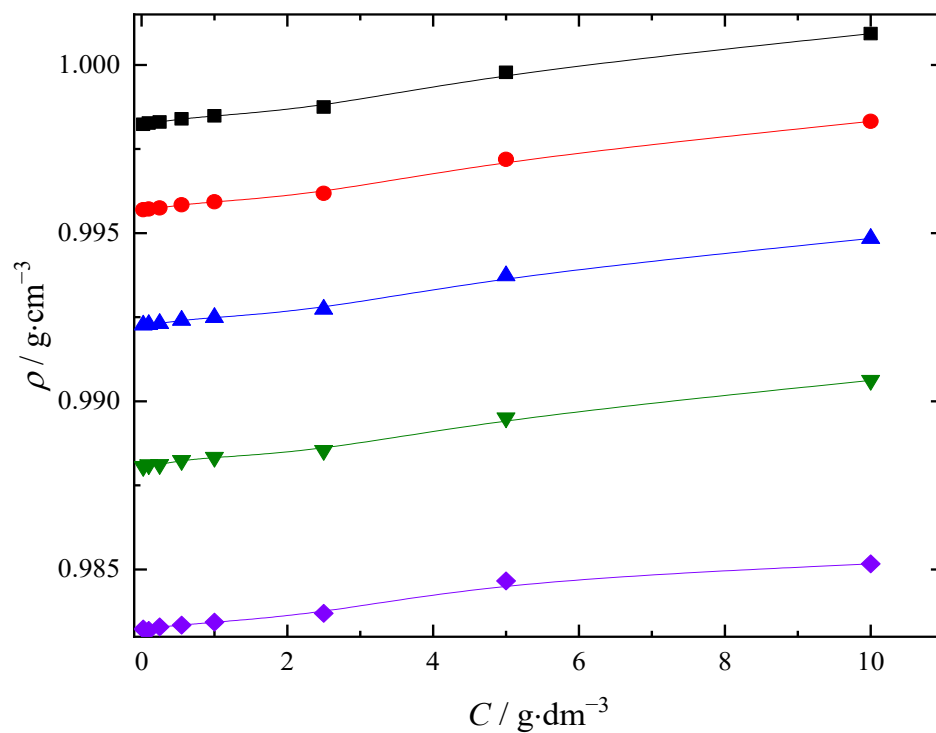


Fig. 7. Density concentration dependence of substance (a) aqueous solution at (\square) 293.15 K, (\circ) 303.15 K, (\triangle) 313.15 K, (∇) 323.15 K, (\diamond) 333.15 K.

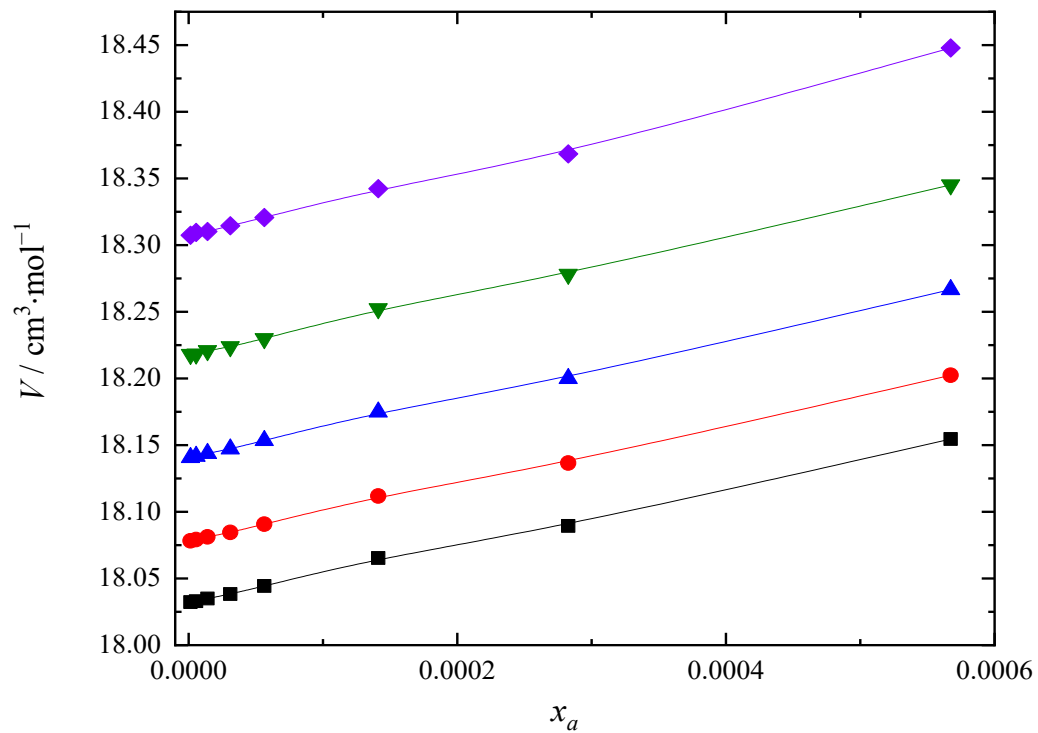


Fig. 8. Average molar volume (\bar{V}) concentration dependence of substance (a) aqueous solution at (\square) 293.15 K, (\circ) 303.15 K, (\triangle) 313.15 K, (∇) 323.15 K, (\diamond) 333.15 K. x_a is a molar fraction of substance (a).

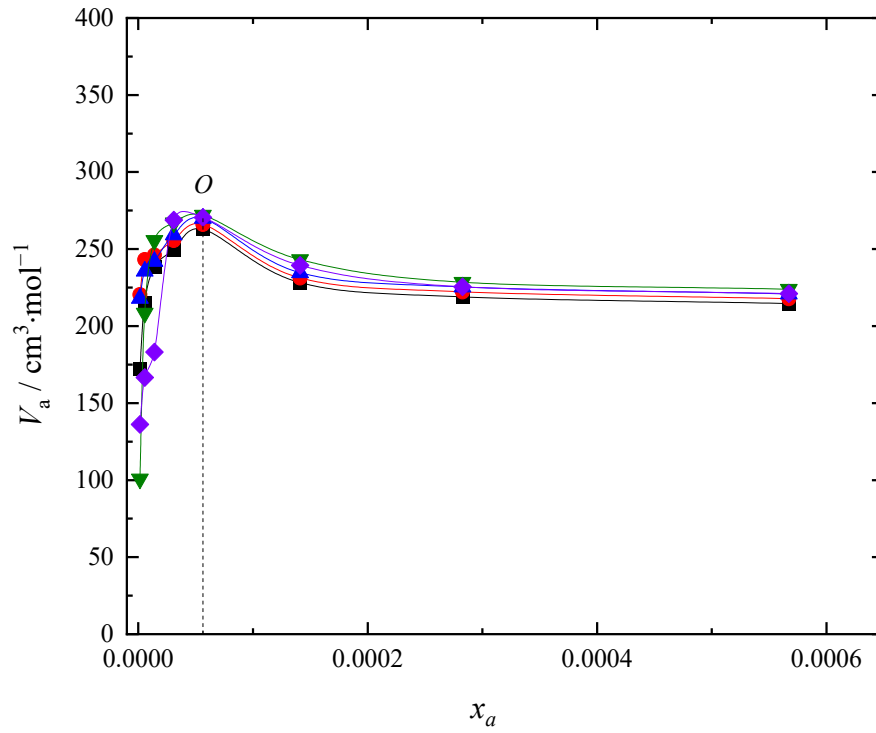


Fig. 9. $\left(\frac{\partial V}{\partial x_a}\right)_{T,P}$ derivative concentration dependence at (\square) 293.15 K, (\circ) 303.15 K, (\triangle) 313.15

K, (∇) 323.15 K, (\diamond) and 333.15 K. O is the extremum point $\left(\frac{\partial^2 V}{\partial x^2}\right)_{T,P} = 0$, $x = 5.3 \cdot 10^{-6}$.

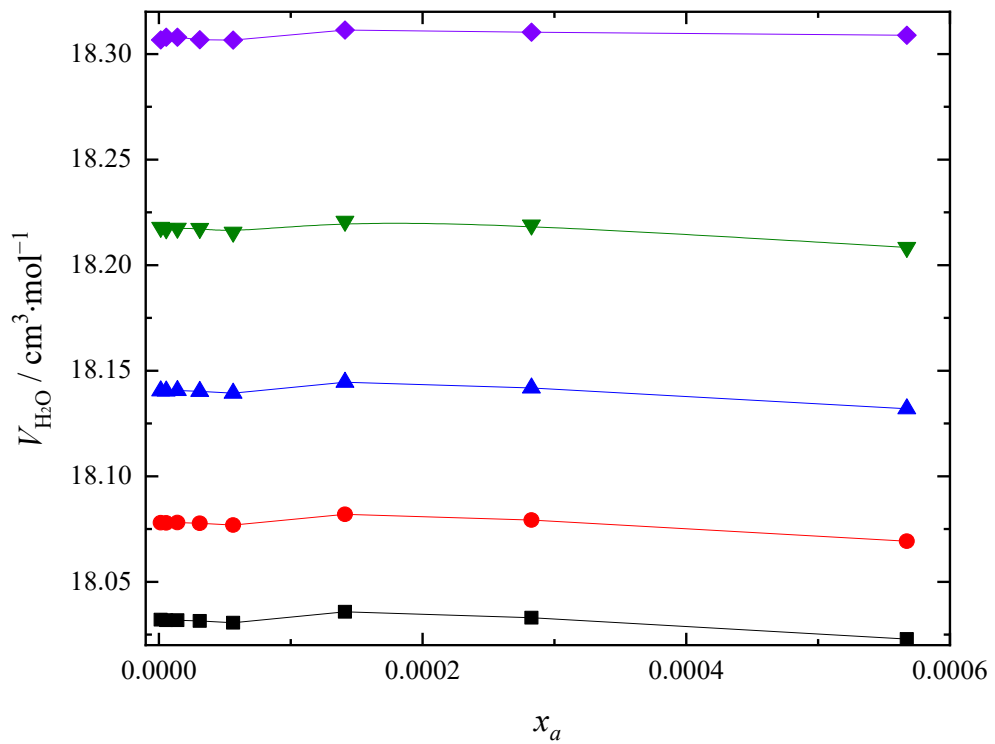


Fig. 10. Water partial volume concentration (x_a) dependence at different temperatures: (□) 293.15 K, (○) 303.15 K, (△) 313.15 K, (▽) 323.15 K, (◇) 333.15 K.

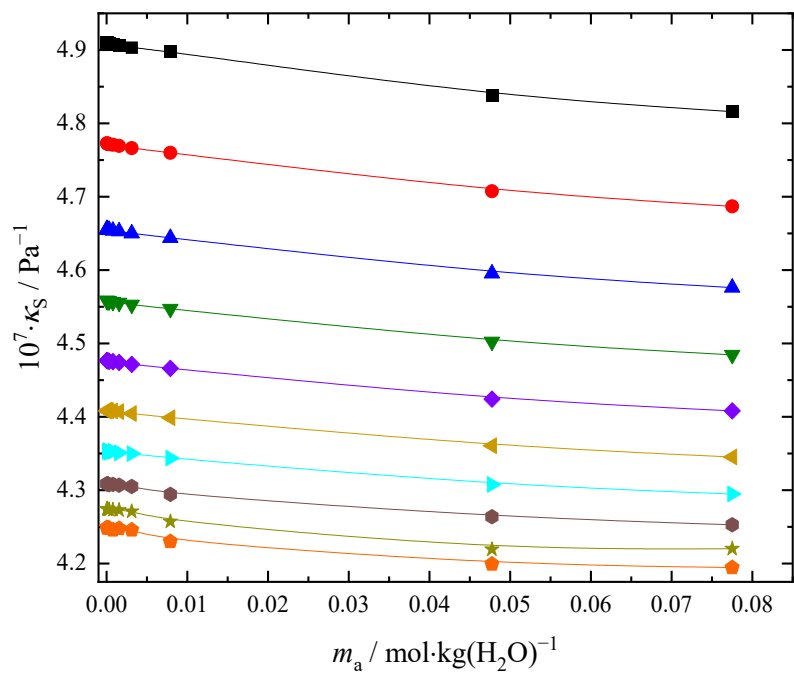


Fig. 11. Isentropic compressibility concentration dependence of substance (a) aqueous solution at (■) 278.15 K, (●) 283.15 K, (▲) 288.15 K, (▼) 293.15 K, (◆) 298.15 K, (◄) 303.15 K, (►) 308.15 K, (●) 313.15 K, (★) 318.15 K, (◆) 323.15 K. m is molality of substance (a).

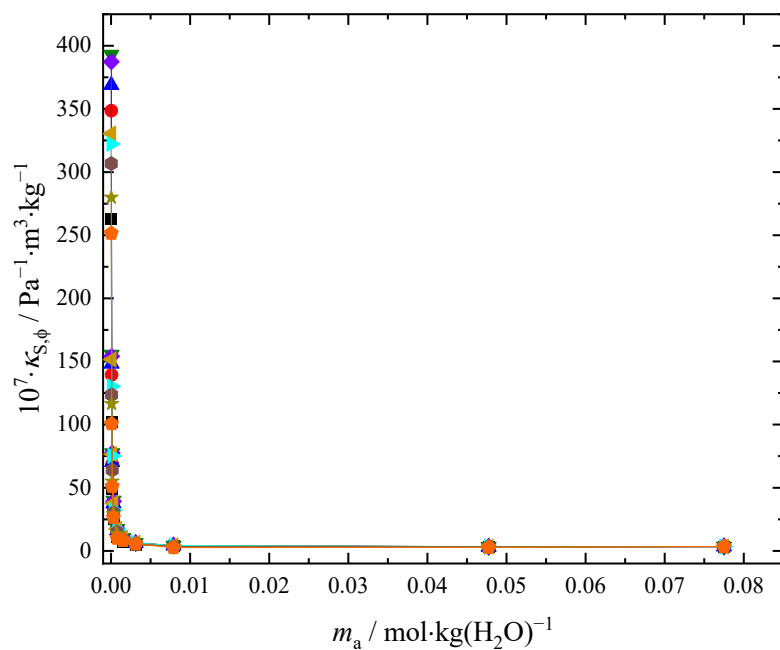


Fig. 12. Apparent specific isentropic compressibility concentration dependence of substance (a) aqueous solution at (■) 278.15 K, (●) 283.15 K, (▲) 288.15 K, (▼) 293.15 K, (◆) 298.15 K, (◄) 303.15 K, (►) 308.15 K, (●) 313.15 K, (★) 318.15 K, (◆) 323.15 K.

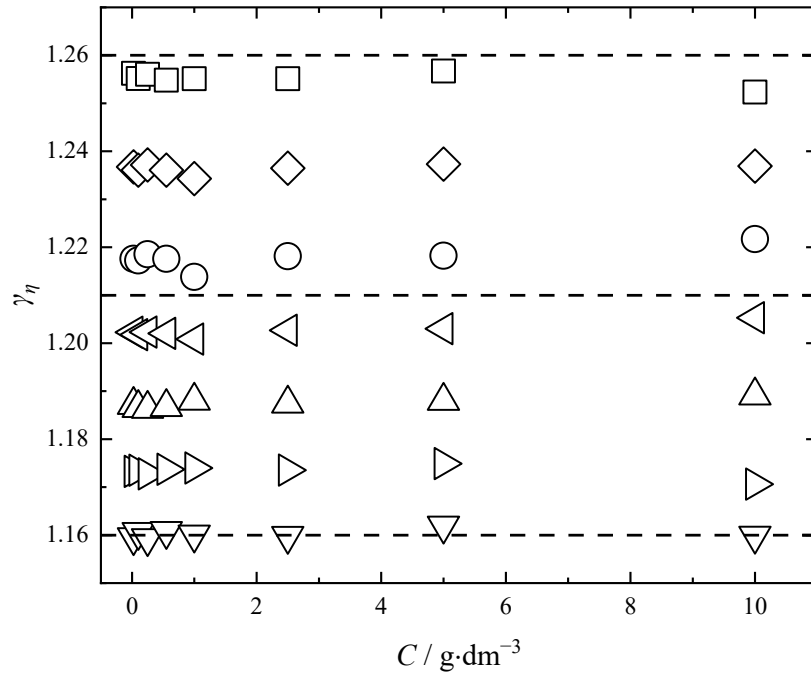


Fig. 13. Van't Hoff viscosity coefficient concentration dependence in substance (a) aqueous

solutions. $(\square) \frac{\eta_{278.15}}{\eta_{288.15}}$, $(\circ) \frac{\eta_{283.15}}{\eta_{293.15}}$, $(\triangle) \frac{\eta_{288.15}}{\eta_{298.15}}$, $(\nabla) \frac{\eta_{293.15}}{\eta_{303.15}}$, $(\diamond) \frac{\eta_{298.15}}{\eta_{308.15}}$, $(\triangleleft) \frac{\eta_{303.15}}{\eta_{313.15}}$, $(\triangleright) \frac{\eta_{308.15}}{\eta_{318.15}}$, $(\hexagon) \frac{\eta_{313.15}}{\eta_{323.15}}$.

$$\frac{\eta_{313.15}}{\eta_{323.15}}$$

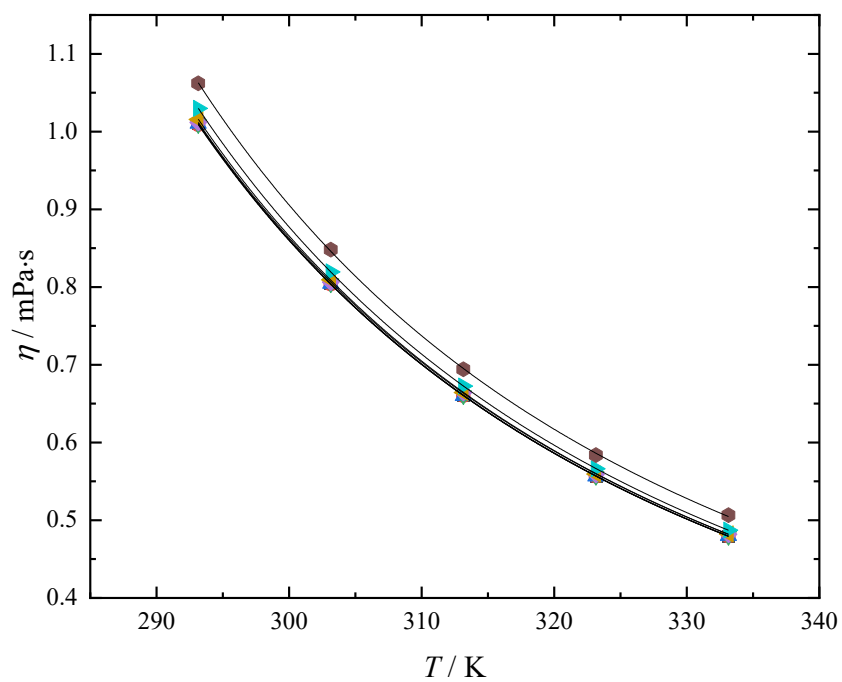
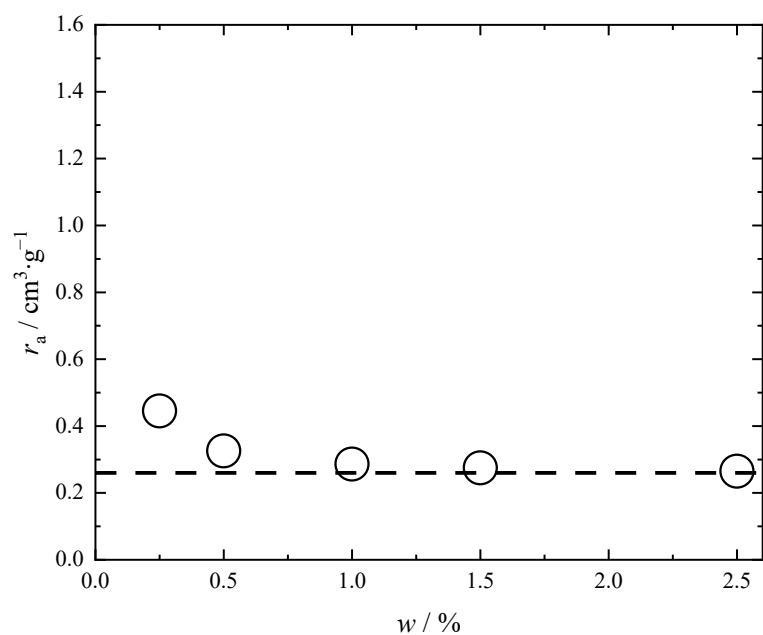


Fig. 14. Dynamic viscosity temperature dependences with a shear rate of 100 s^{-1} of substance (a) aqueous solutions at $C = (\square) 0.1 \text{ g}\cdot\text{dm}^{-3}$, $(\circ) 0.25 \text{ g}\cdot\text{dm}^{-3}$, $(\triangle) 0.5 \text{ g}\cdot\text{dm}^{-3}$, $(\nabla) 1 \text{ g}\cdot\text{dm}^{-3}$, $(\diamond) 2.5 \text{ g}\cdot\text{dm}^{-3}$, $(\triangleleft) 5 \text{ g}\cdot\text{dm}^{-3}$, $(\triangleright) 10 \text{ g}\cdot\text{dm}^{-3}$, $(\odot) 15 \text{ g}\cdot\text{dm}^{-3}$.

(a)



(b)

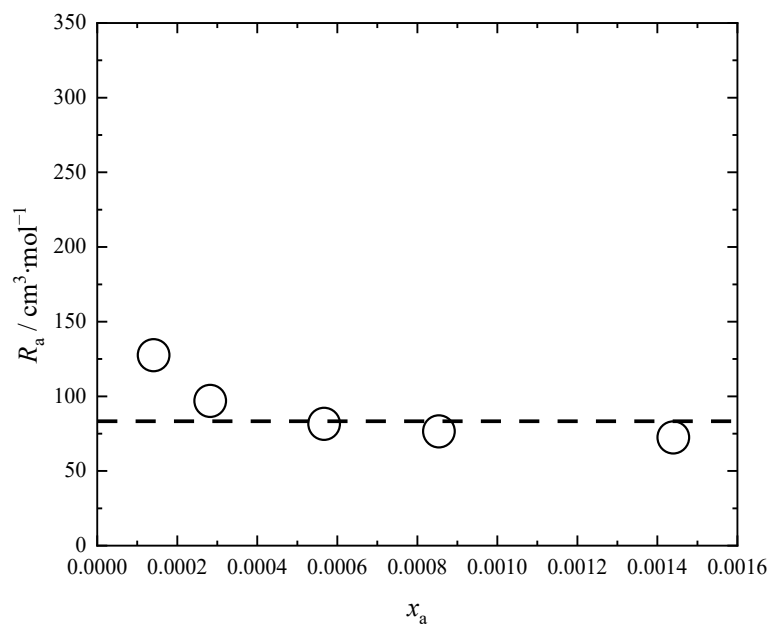
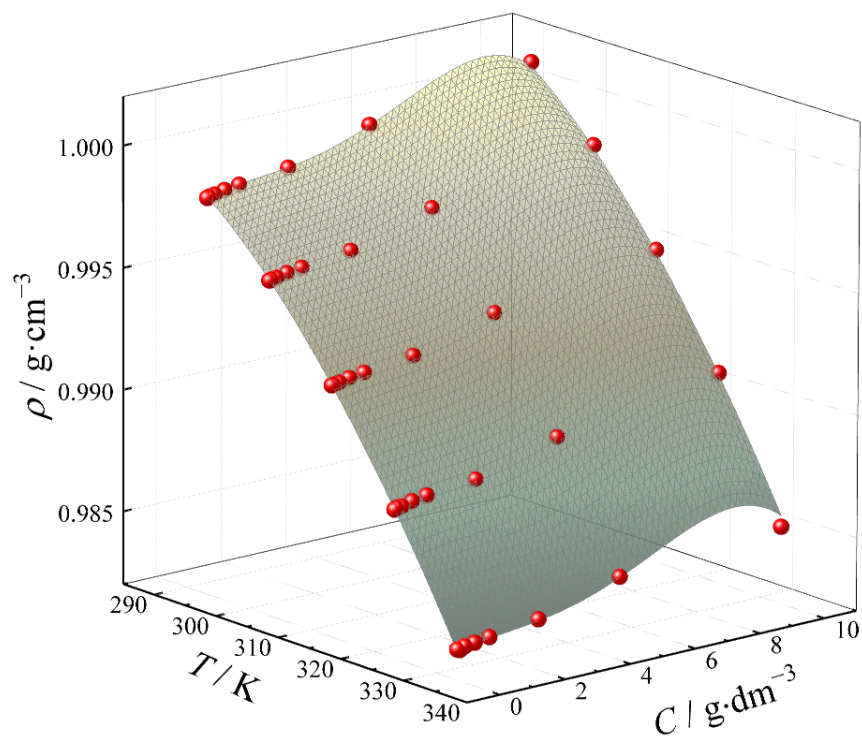
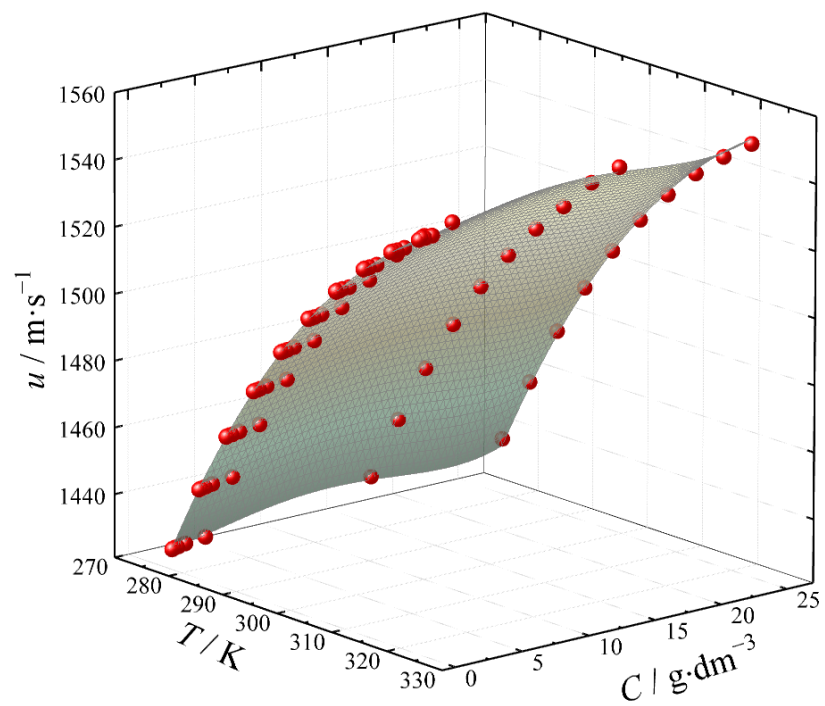


Fig. 15. Specific (a) and molar (b) refractions concentration dependence in aqueous solutions at 293.15 K. w is the mass fraction of substance (a), x_a is the molar fraction of substance (a).

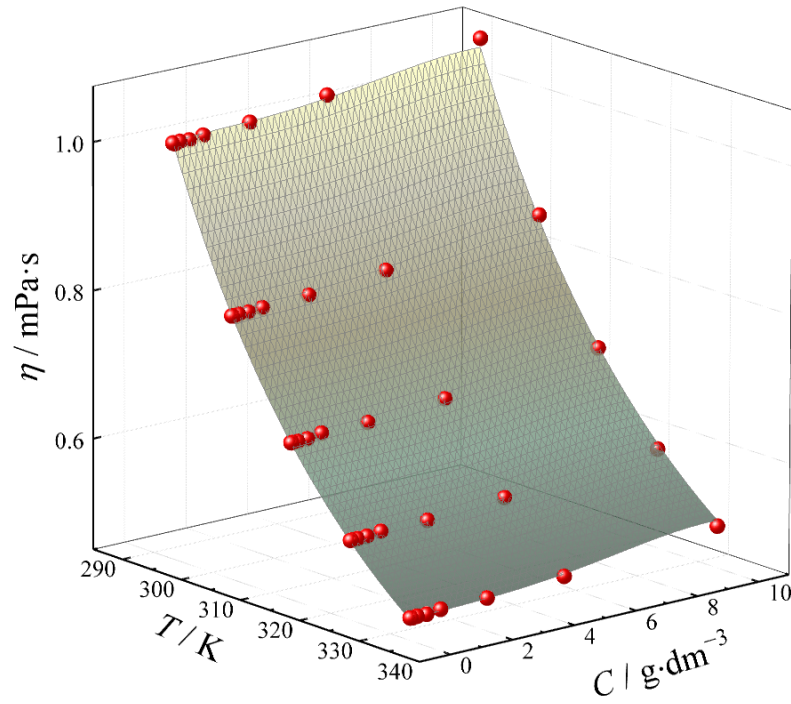
(a)



(b)



(c)



(d)

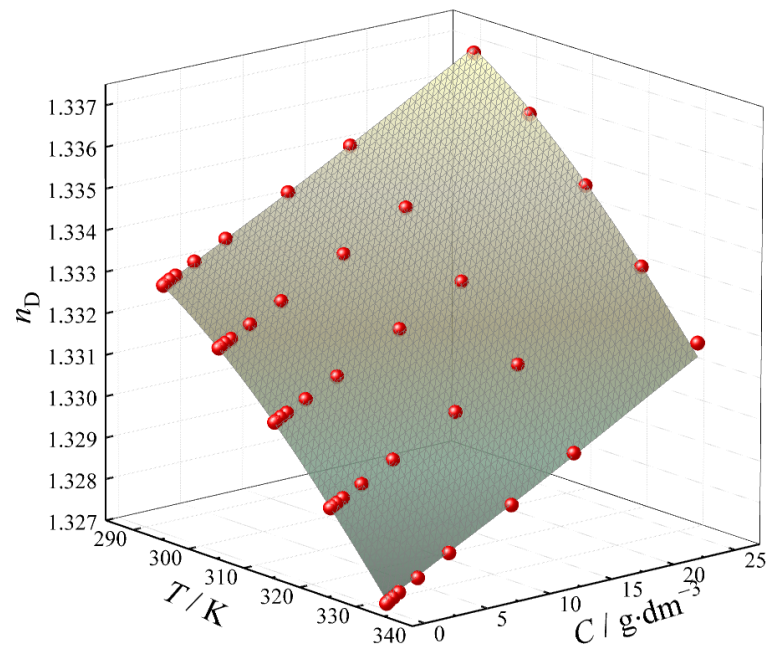


Fig. 16. T - C dependences of substance (a) aqueous solutions density (a), speed of sound (b), dynamic viscosity (c), refractive index (d). Spheres are experimental data; surfaces are calculated data.

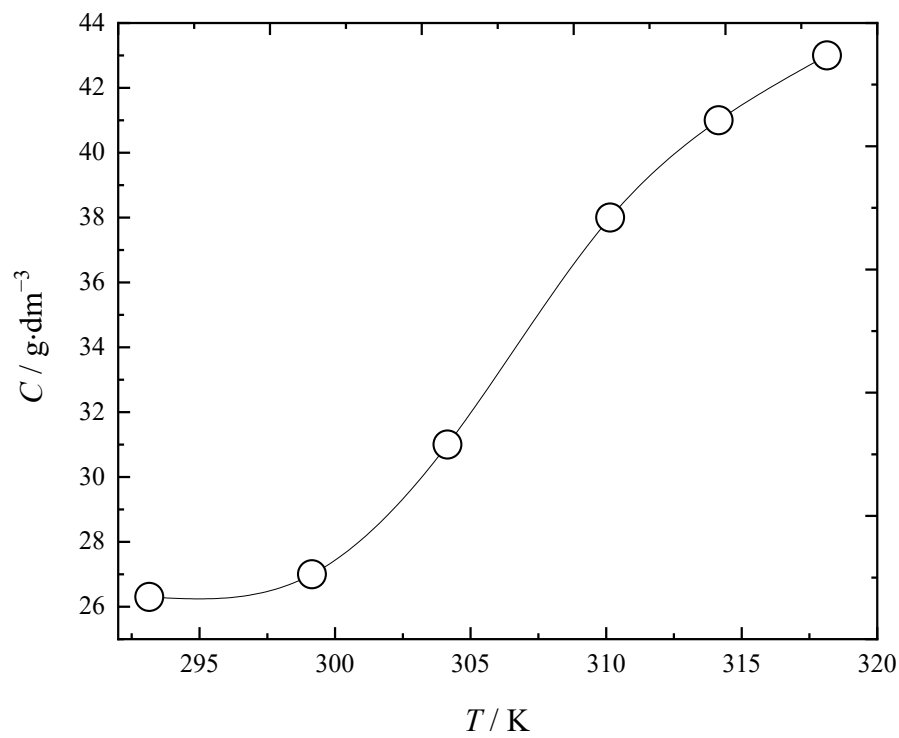


Fig. 17. Polythermal solubility of substance (a).

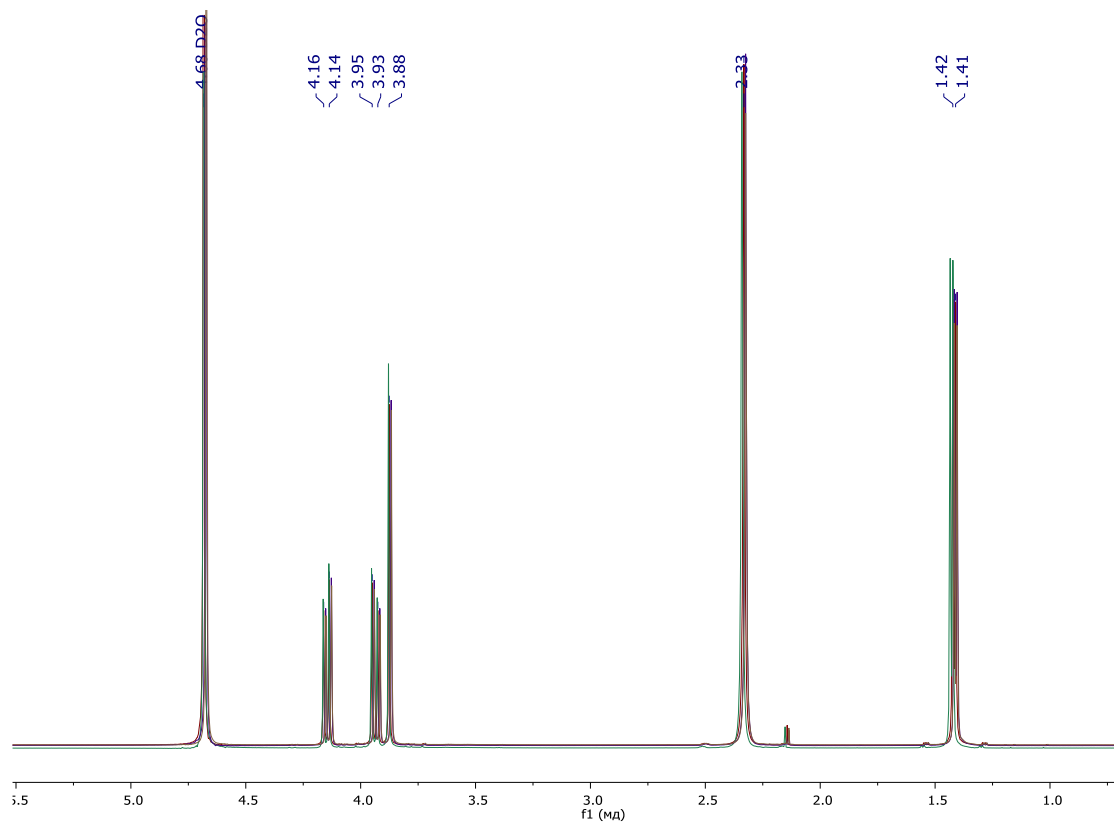


Fig. 18. ^1H NMR spectra of substance (a) in D_2O after 24 h (pink), 20 h (blue), 16 h (green) and 12 h (red).

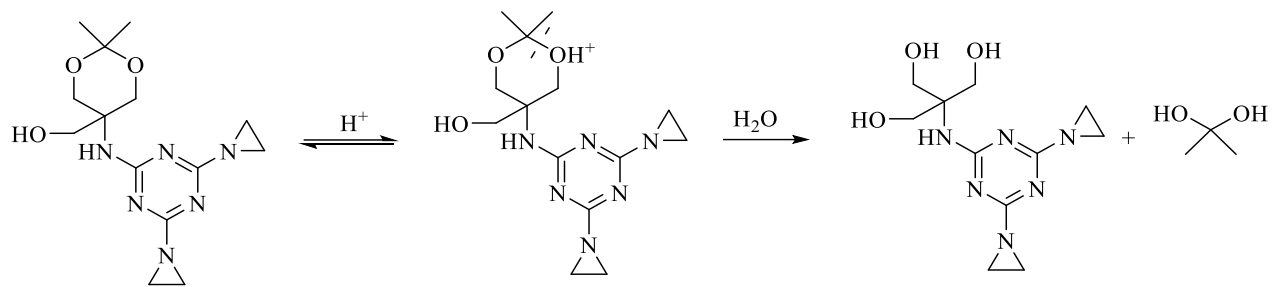


Fig. 19. Hydrolysis scheme of substance (a).

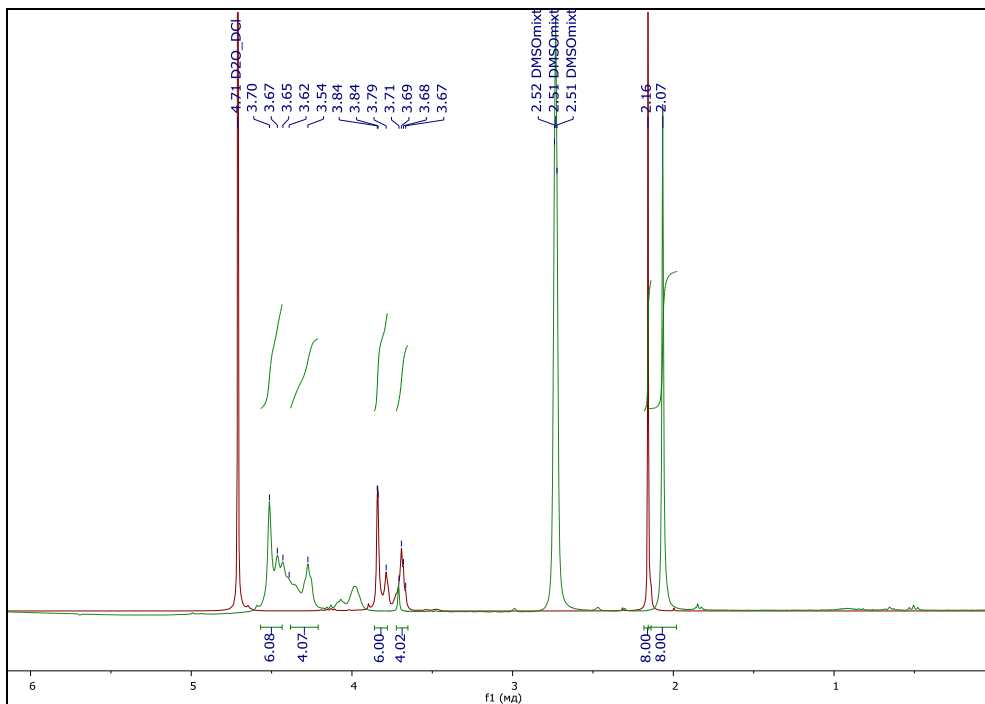


Fig. 20. ¹H NMR spectra after hydrolysis of substance (a) at pH = 3 (red) and pH = 4 (green).

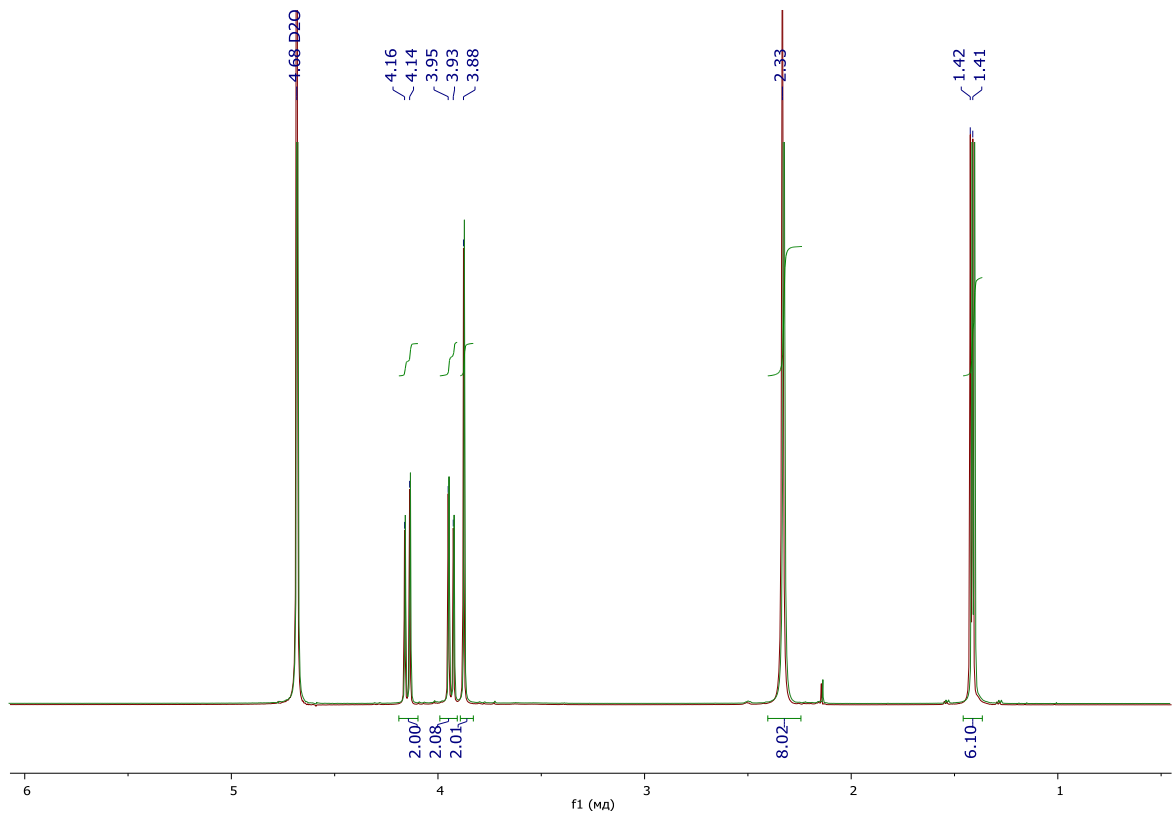


Fig. 21. ^1H NMR spectra of substance (a) in D_2O (red) and at $\text{pH} = 10$ (green).

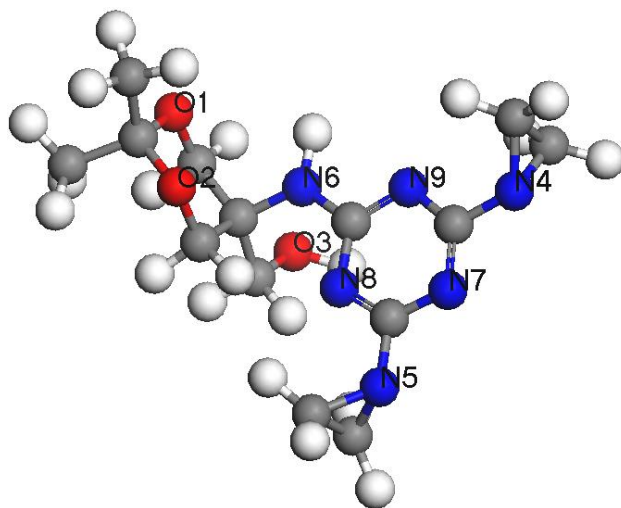


Fig. 22. Structure of substance (a) with allocated oxygen and nitrogen atoms.

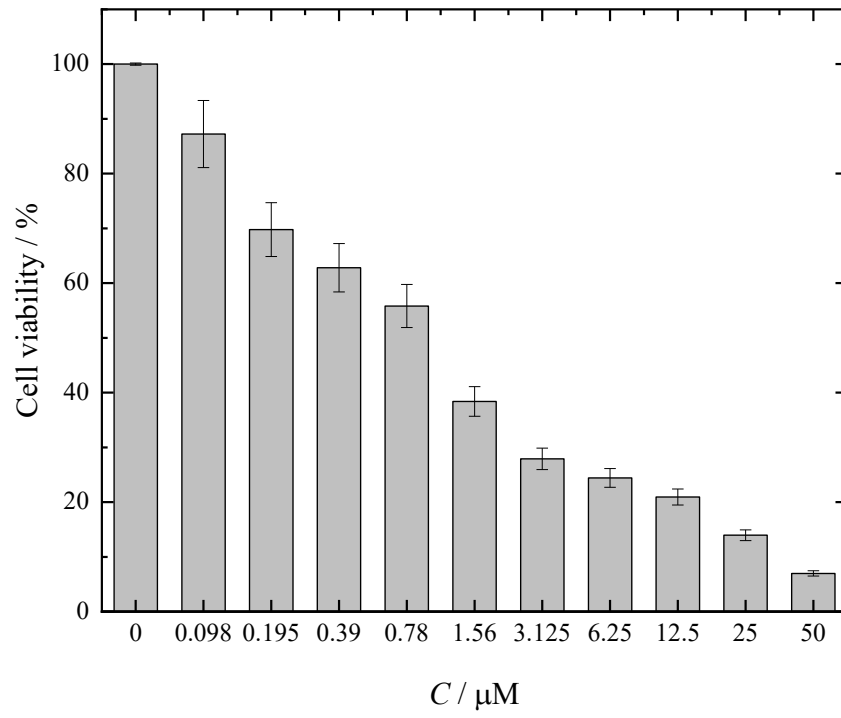


Fig. 23. Effect of substance (a) on Capan-2 cell line viability.

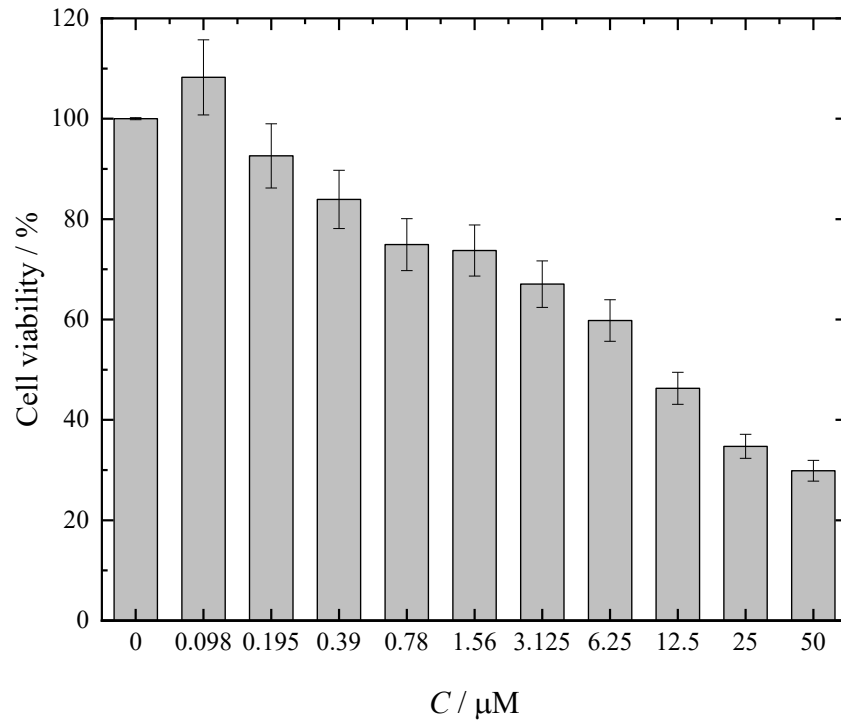


Fig. 24. Effect of substance (a) on SK-MEL-1 cell line viability.

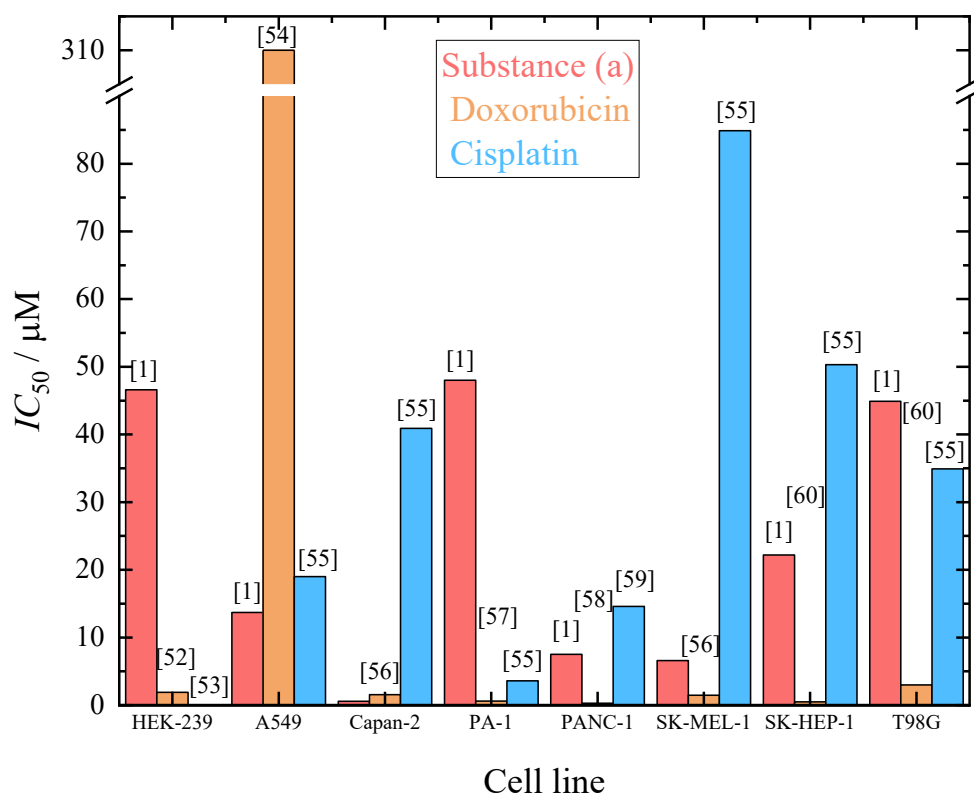


Fig. 25. Comparison of IC_{50} values of substance (a) (left column), doxorubicin (middle column), and cisplatin (right column) for the following cell lines: HEK293, A549, Capan-2, PA-1, PANC-1, SH-MEL-1, SK-HEP-1, and T98G. Columns with numbers indicate literature data references [1,52–60].

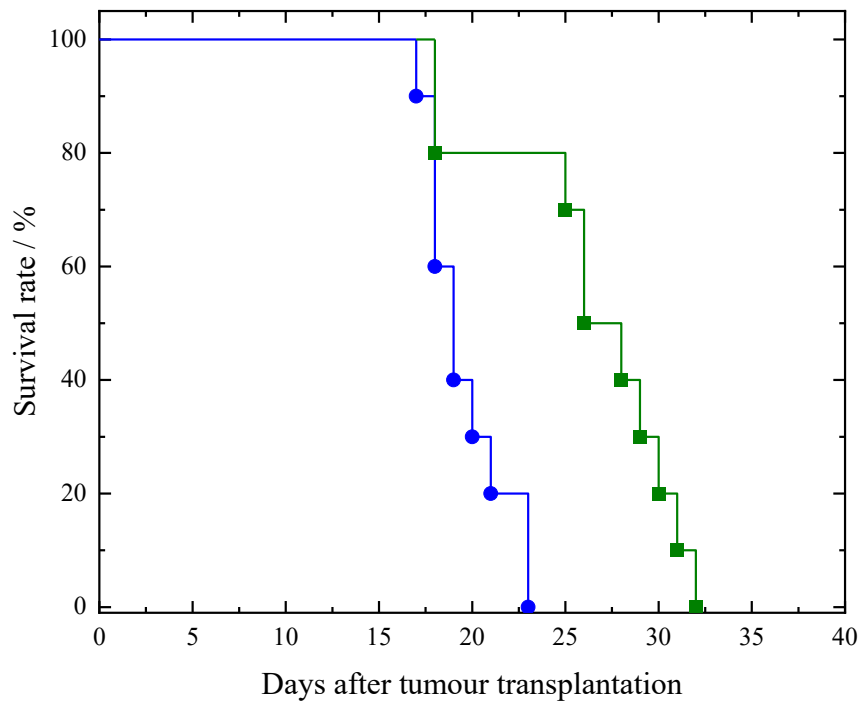


Fig. 26. Effect of substance (a) on the survival of mice with Ehrlich ascites carcinoma, where ○ marks the control group and □ marks the substance (a) group.